# MOLECULAR DYNAMICS SIMULATION OF THE FULLY HYDRATED DIPALMITOYLPHOSPHATIDYLCHOLINE (DPPC) BILAYER



SURAJITH NALANTHA WANASUNDARA

# NOTE TO USERS

# MOLECULAR DYNAMICS SIMULATION OF THE FULLY HYDRATED DIPALMITOYLPHOSPHATIDYLCHOLINE (DPPC) BILAYER

By

© SURAJITH NALANTHA WANASUNDARA

A THESIS SUBMITTED TO THE SCHOOL OF GRADUATE STUDIES
IN PARTIAL FULFILLMENT OF THE REQUIRMENTS FOR THE DEGREE OF
**MASTER OF SCIENCE**

COMPUTATIONAL SCIENCE
MEMORIAL UNIVERSITY OF NEWFOUNDLAND
DECEMBER 2003

ST. JOHN'S NEWFOUNDLAND

*Your file Votre référence*
*ISBN: 0-612-99127-X*
*Our file Notre référence*
*ISBN: 0-612-99127-X*

# ABSTRACT

The structural properties of lipid bilayers in biological membranes are of great interest in biochemistry, biophysics, and medicine. The main goal of the present study was to use molecular dynamic (MD) techniques to investigate physical properties of the hydrated dipalmitoylphosphatidylcholine (DPPC) bilayer.

The bilayer model consists of 25 DPPC molecules per each monolayer and 44.8% water by total weight. A modified version of AMBER MD suit of programs with CHARMM22 force field for phospholipids was used in simulation. The isothermal-isobaric or NPT ensemble with a fully flexible simulation box in ROAR program was used in this study. Simulations were performed under different pressure and temperature conditions.

According to experimental results, a liquid crystal phase ($L_\alpha$) is expected with the DPPC bilayer simulated under 1 atm pressure and 323 K temperature conditions. However, area per lipid, bilayer thickness, chain tilt, and the order parameters resulting from the present simulation appeared to be more consistent with the known properties of the $L_{\beta'}$ phase. An increase of temperature up to 423 K increased the area per lipid of the bilayer system. Average chain tilt values at 423 K were lower than those at 323 K. Further, ends of alkyl chains showed more disorder at 423 K compared to those at 323 K. Increase of system pressure up to 1000 atm at constant temperature (323 K) decreased the area per lipid while increasing the bilayer thickness compared to the results obtained at 1 atm. Further increase of pressure up to 2000 atm did not change the area per lipid but slightly decreased the bilayer thickness from that of at 1000 atm. Greater ordering was observed with an increase of pressure.

# TABLE OF CONTENTS

# LIST OF FIGURES

## LIST OF TABLES

# ACKNOWLEDGEMENTS

I would like to express my sincere gratitude to Dr. Jolanta Lagowski for her guidance and support throughout the course of my study. Her advice and support in editing of this thesis is also greatly appreciated.

My special thanks goes to Patrick Byrne for constructing the initial bilayer system and writing analytical codes which have been used to analyze data in this study. Special thanks are extended to Fred Perry and Darryl Reid, Computational and Visualization Center, Memorial University of Newfoundland, for their technical assistance and invaluable computing information. I also like to thank Advanced Computing and Visualization Center at the Memorial University and MACI's SGI High Performance Computing complex at The University of Alberta, for providing computer facilities to perform these simulations. I would also like to thank all staff members and graduate students in the Department of Physics and Physical Oceanography and Computational Science program, my wife and all my friends for their help and encouragement throughout my studies.

Financial support provided through my M.Sc. studies by the Natural Sciences and Engineering Research Council (NSERC) and the School of Graduate studies were also greatly appreciated.

# Chapter 1

# INTRODUCTION

## 1.1 MOLECULAR DYNAMICS SIMULATION

Molecular dynamics simulation techniques are used to study the dynamics of individual molecules in models of solids, liquids, and gases, i.e., they study how their positions, velocities, and orientations change with time [1]. The molecular dynamics method was first introduced by Wainwright (Alder and Wainwright, 1957, 1959) [2,3] to study the interactions of hard spheres [4]. Stillinger and Rahman (1974) [5] were credited in performing the first simulation of a realistic system using a liquid water system. Many new algorithms were produced in the 1980s in part due to the introduction of modifications to the equations of motion in classical mechanics [6]. These modifications allowed the adaptation of the computer simulations to various situations. Today, molecular dynamics simulation methods are used in studying solvated proteins, protein-DNA complexes as well as lipid systems addressing a variety of issues including the thermodynamics of ligand binding and the folding of small proteins.

In general, in a computer simulation, if the chosen model is a suitable one, and then it can be used to get insights to assist in the interpretation of theoretical results. It also provides a direct route from the microscopic details of a system (the size and number of

atoms, the interaction between them, molecular geometry, etc.) to macroscopic properties of an experimental interest (the equation of state, phase diagrams, transport coefficients, etc.). The dual role of simulation, as a bridge between models and theoretical predictions on the one hand, and between models and experimental results on the other, is illustrated in Figure 1.1.

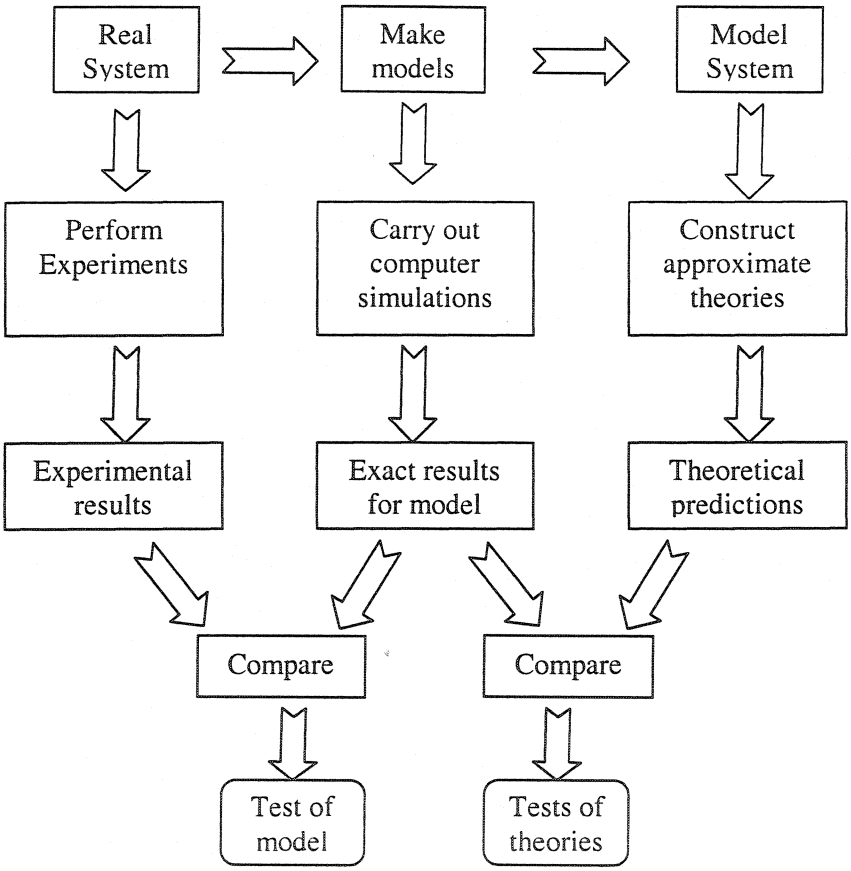


Figure 1.1: The connection between experiment, theory, and computer simulation [7]

Results from computer simulation is academically and technologically important in cases where it may be difficult or impossible to carry out experiments under extremes of

temperature and pressure and also to understand multi-component models and their complex interrelationships. Considerable advances in the field of computer simulation of molecular systems have taken place with the improvements in computer hardware and the wider availability of simulation software [8].

The three most common types of computer simulation are: discrete event, continuous and Monte Carlo [9]. Computer simulation techniques can also be divided into three classes: knowledge or rule based methods, quantum mechanical methods, and classical 'potential energy' based techniques [8]. These three areas are not mutually exclusive and it may be necessary to combine them sometimes to tackle particular problems. Some of the general-purpose computer simulation programs available to study molecular dynamics are AMBER [10], CHARMM [11], GROMOS [12] and OPLS [13].

## 1.2 PHOSPHOLIPIDS AND BIOLOGICAL MEMBRANES

All living cells have a membrane that separates the cell interior from the surroundings. Membranes also envelop many of the cell components such as mitochondria and chloroplasts. Biomembranes serve as a barrier to maintain the integrity of cells, and also provide the functional environment for a large number of proteins [14]. Phospholipids are the major structural elements of biological membranes, while globular proteins may be inserted into the bilayer in a random fashion (Figure 1.2). Figure 1.2 depicts the current conception of the fluid mosaic model of a biological membrane at one point in space and time as the entire structure is thought to be dynamic with most components capable of rotational diffusion.

The role of phospholipids in biological membranes is closely related to their ability to form bilayers when dispersed in water [15]. The phospholipid molecule is composed of two apolar hydrocarbon chains and one polar phosphate-containing head group attached to a glycerol backbone (Figure 1.3).

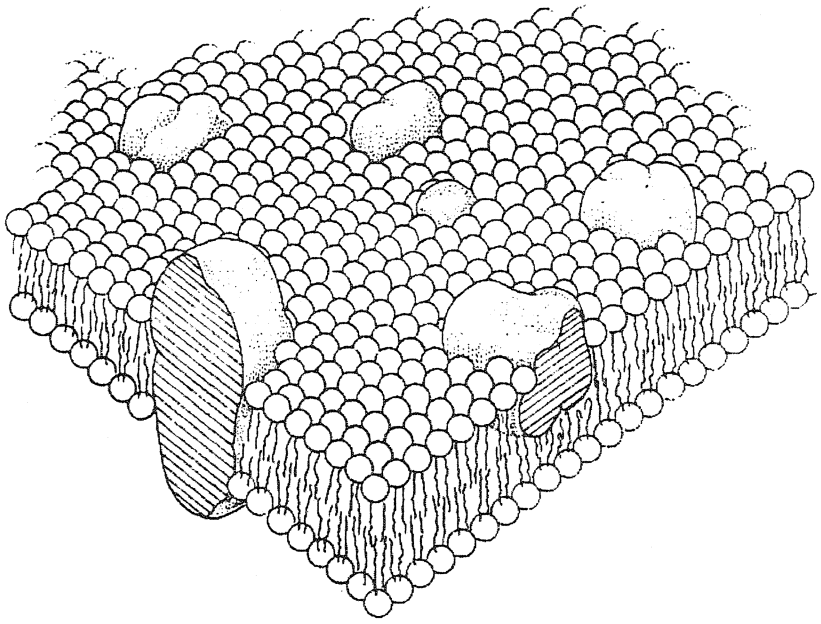

Figure 1.2 The lipid-globular protein mosaic model of a biological membrane with a lipid matrix [16]

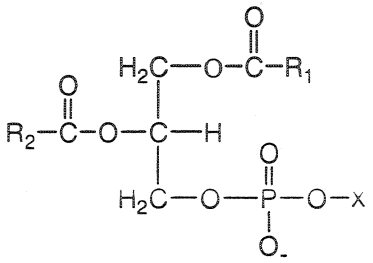


$R_1$ and $R_2$: Alkyl chains

Figure 1.3: General structural formula of glycerophospholipids. X is an alcohol that is esterified on to the phosphate headgroup. [15]

The nonpolar hydrocarbon chains dislike the polar aqueous environment when phospholipids contact with water and they stick together pointing their polar heads to the outside of the aggregates (Figure 1.4). The polar head groups can be stabilized by ion-dipole and H-bonds between charged head groups and water. Repulsive forces may also be involved. Head groups can repel each other through steric factors, or ion-ion repulsion from like-charged head groups. The attractive forces must be greater than the repulsive forces, which lead to the formation of these molecular aggregates. Due to the specific shape of most lipid molecules, bilayers are the favored structure rather than micelles or inverted hexagonal phases [15].

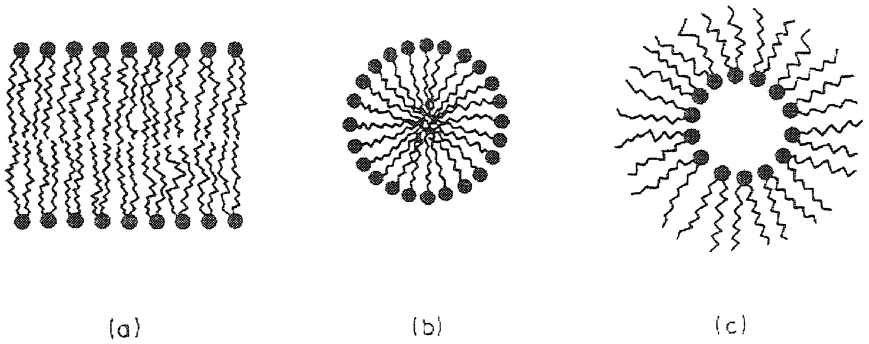


Figure 1.4: States of aggregation of phospholipids in water: (a) bilayer, (b) micelle, and (c) inverted cylinders [15]

The hydrocarbon chains in phospholipids may vary in length but are usually between twelve and sixteen alkyl groups long [17]. Further, the alkyl chains can be saturated or unsaturated. The polar groups may also vary, from the zwitterionic phospholipids (e.g. phospatidylcholine) to charged molecules (e.g. phosphatidylinositol)

[18]. The most prevalent molecule that forms the bilayer of eukaryotic cell membranes is phosphatidylcholine (PC) [19]. The dipalmitoylphosphatidylcholine (DPPC) molecule, which was used to build the bilayer model for the present work, consists of two saturated 16-carbon fatty acid chains connected by a glycerol backbone with a zwitterionic head group (Figure 1.5).

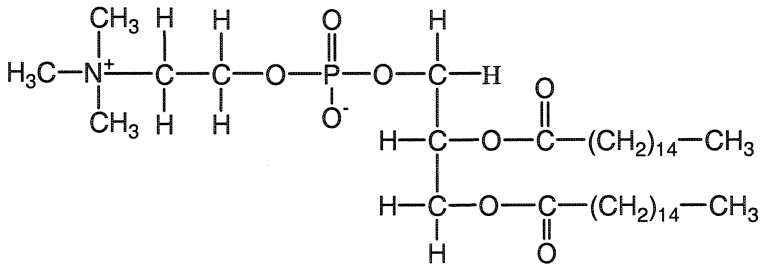

Figure 1.5: DPPC molecule

## 1.3 PHASE BEHAVIOUR OF PHOSPHOLIPIDS

Dry amphiphiles and hydrated lipids at relatively low temperatures typically form densely packed crystalline structures, named as crystal or $L_c$ phase [17]. For binary lipid-water systems, the amphiphilic nature of the phospholipid molecule allows it to form a variety of different structures and phases with the increase of temperature and/or water content in the system (Figure 1.6).

At some subtransition temperature, the two-dimentional lipid crystal normally transforms into a more expanded lipid gel phase of the $\beta'$ or, more frequently, $\beta$, organization with tilted or untilted chains, respectively [17]. Increasing hydration may lower the phospholipid subtransition temperature. Lipid chains in the gel state are packed

on a (skewed) hexagonal lattice and are moderately tilted ($L_{\beta'}$) or untilted ($L_{\beta}$). Some phospholipids such as DPPC form only a $L_{\beta'}$ phase at subtransition temperature. Heating lipids above the subtransition temperature enhances the torsional oscillations of the hydrocarbon chains until these turn into essentially unhindered long-axis rotation. Some lipids display a pretransition at which the lipid head group mobility and the interfacial area per molecule increase. The bilayer surfaces at such a pretransition temperature break up into a series of periodic, asymmetric, quasi-lamellar bilayer segments that give rise to the appearance of the surface undulations or ripples characteristic of the $P_{\beta'}$ or $P_{\beta}$ phase. As temperature of the bilayer system increase further, it undergoes a phase transition to the liquid crystal ($L_{\alpha}$) phase (in general, at fixed temperatures, an increase in hydration does not lead to phase transitions). In $L_{\alpha}$ phase bilayers, the lipid molecules move much more freely and may even undergo lateral diffusion throughout the bilayer. As well, the hydrocarbon chains become more fluid in nature. For this reason, the transition between a gel phase and the $L_{\alpha}$ phase is often referred to as a chain melting transition [15]. Schematic representation of a phospholipid bilayer undergoing a phase transition from the more rigid crystalline state to the more random fluid state is shown in Figure 1.7.

The gel-to–fluid phase transition is believed to have a substantial effect on membrane function. Living organisms try to keep their membrane bilayers close to a fluid-phase optimum, either by means of chemical chain modifications or by synthesizing appropriate soluble molecules [17]. This appears to be necessary because such processes

as membrane biogenesis, transmembrane transport, and exo- and endocytosis can only occur when the membrane exhibits sufficient fluidity [16].

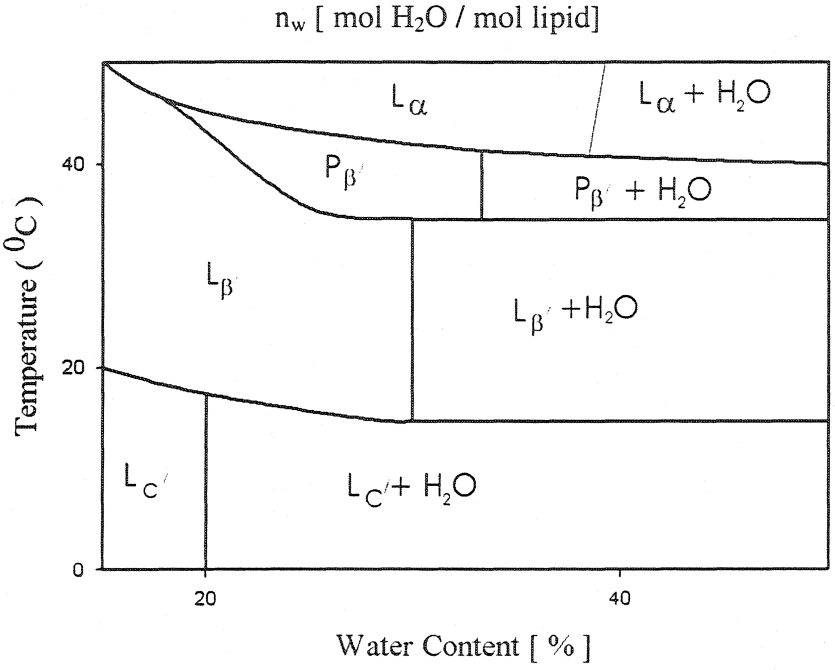


Figure 1.6: Partial phase diagram of DPPC in water [Based on reference 17]

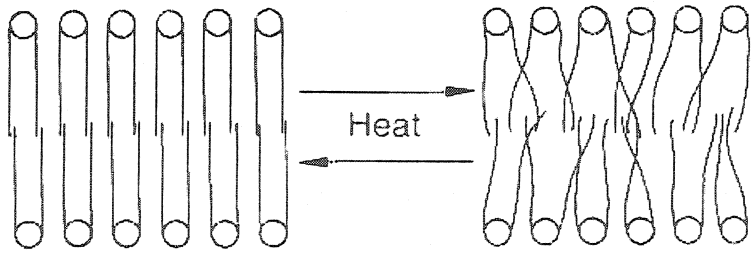


Figure 1.7: Schematic representation of a phospholipid bilayer undergoing a phase transition from the more rigid crystalline state to the more random fluid state [16]

Wong *et al.* (1987) [20] have shown the existence of five pressure-induced gel phases of the DPPC bilayer through Raman and Infrared spectroscopic analyses. The lipid bilayer structure in each of the five gel phases (named GI through GV corresponding to the increasing pressure of the transition) and the liquid crystal phase ($L_\alpha$) of DPPC are shown in Figure 1.8.

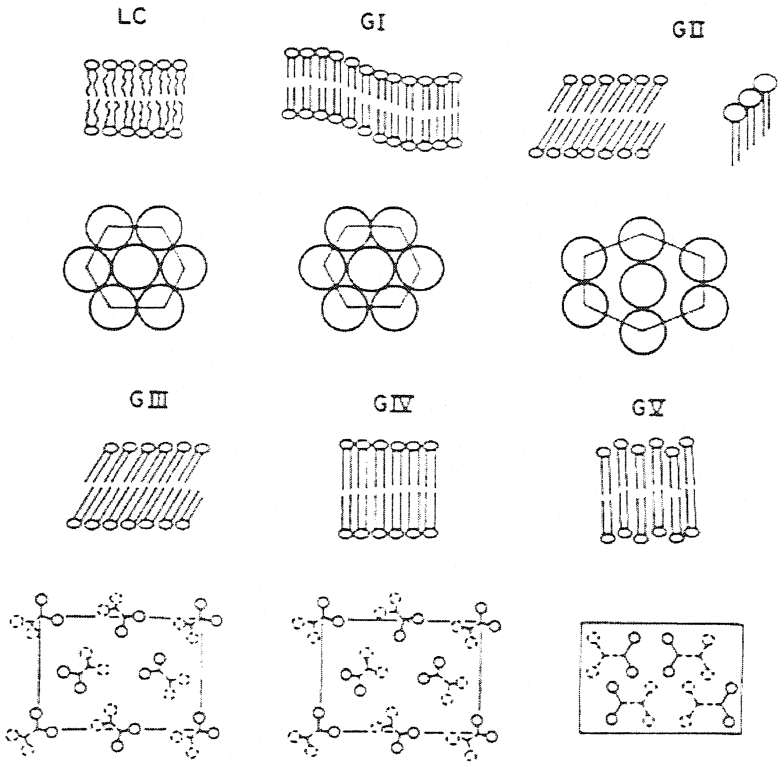


Figure 1.8: Representations of the lipid packing and interchain structure in the liquid crystal and GI-GV gel phases of DPPC [20]

The GI and GII phases in this study refer to $P_{\beta'}$ and $L_\beta$ phases described earlier, respectively. However, the structure and dynamics of GIII, IV and V are not well studied by other methods. In addition to Wong's studies, small angle neutron diffraction [21, 22]

has shown the existence of a pressure induced interdigitated phase in DPPC bilayers at pressure above 1 kbar and temperatures above 40°C. High-pressure phases of DPPC have also been studied by using deuterium NMR [23]. Figure 1.9 illustrates the pressure/temperature phase diagram of a 15 % (by wt.) dispersion of DPPC in water.

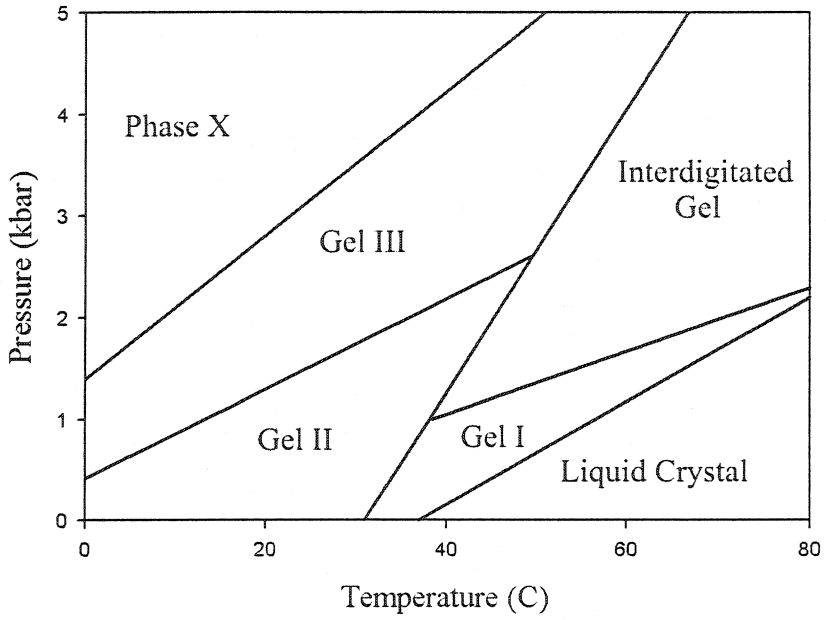


Figure 1.9: Pressure/temperature phase diagram of DPPC (15 % by wt. in water) [Based on reference 23]

## 1.4 COMPUTER SIMULATION STUDIES OF LIPID BILAYERS

Understanding lipid bilayers and proteins in biological membranes from the atomic point of view is of great biochemical, biophysical, and medical interest. A better understanding of the structure and dynamics of membranes and membrane proteins may help in the development of pharmaceuticals, anesthetics, and drug-delivery agents [24].

Furthermore, studies of pure membrane structural and dynamical properties at the atomic level can enhance our understanding of more complicated biological membrane functions and their environmental interactions.

The time scales of biochemically relevant fluctuations in membranes can span anywhere from femtoseconds ($10^{-15}$s), for intramolecular vibrations, to minutes or hours ($10^{3}$s), for lipid molecule transbilayer flips (Blume, 1993) [25]. Further, motion can occur on different length scales (from 0.01 Å up to 100 Å) and on different energies (0.1-100 kcal/mol) [26]. Phospholipid bilayers are used as models to study the characteristics of biological membranes. Some important dynamic properties of membranes are lateral diffusion of lipids within a lipid membrane, dynamical fluctuations within a lipid moiety (rotational, reorientation, and relaxation), *gauche-trans* equilibrium, and their respective interconversions [24]. However, little atomic-level structural data is available even for single-component membranes due to very fluid and dynamical structures of phospholipid bilayers under physiologically relevant conditions of temperature and hydration [27, 28, 29]. Methods such as nuclear magnetic resonance (NMR) spectroscopy, neutron diffraction, X-ray diffraction, Raman spectroscopy, etc. have been used to obtain the experimental data available on lipid bilayers [30]. However, spectroscopic measurements provide information averaged over the time scale of the experiment and the fine details of the molecular motion are not directly measured if the motion is fast relative to the experimental time scale (Brooks et. al., 1988) [31]. Due to these reasons, theoretical methods such as molecular dynamics calculations have become a powerful tool in studying structural and dynamical properties in membranes at atomic level. Most of the

molecular dynamics studies on lipid bilayers have been performed at constant number of atoms, volume, and temperature (NVT, or canonical) [32, 33, 34], or at constant number of atoms, pressure, and temperature (NPT) conditions [35, 36, 37].

First molecular dynamics simulation study of lipid bilayer was reported by Ploeg and Berendsen (1980, 1982) [38, 39]. They used a small lipid system (2 x 16 decanoate molecules) to represent biological membrane. Periodic boundary conditions together with the small system size gave rise to artifacts with this study. Thus, the system size was increased to 2 x 64 decanoate molecules in later studies by the same group [40]. Since then, many other investigations with increased sophistication and system size have been carried out. For example, simulation of complete lipid molecules (2 x 24 1,2-dimyristoyl-*sn*-glycero-3-phosphatidylethanolamine (DMPE) molecules and 553 water molecules) [41] made the model more realistic. An important improvement was the inclusion of water and ions in the simulation [42]. The first simulation of a phospholipid bilayer including water molecules was done by Egberts in 1988 (PhD thesis) and published in 1994 as an article [43]. After that, substantial simulation researches have been performed on phospholipid bilayers of DPPC [35, 36, 44, 45], DMPC [24, 37, 46], POPC (palmitoyloleoylphosphatidylcholine) [19], DLPE (dilaureoylphosphatidylethanol -amine) [47], and so on.

With the improvements in computer software and the model systems used, molecular dynamics studies of lipid bilayers at present perform well in terms of reproducing structural parameters such as bilayer thickness [19], cross-sectional area per lipid [19, 30, 37, 48], and so on. Dynamic properties, such as permeation rates for small

molecules passing through a membrane, have also been reasonably well reproduced considering some of the approximations used in those simulations [49, 50]. However, two limitations still exist when one uses molecular dynamics to probe membrane properties [24]. The first limitation is system size. Typical molecular dynamic simulations seldom span more than 100 Å in any direction of the simulation cell, making it feasible to only treat a few hundred lipid molecules with present-day resources. The second limitation involves the accessible time scales. The current molecular dynamic simulations seldom span more than a few nanoseconds, with simulations of 10 or more nanoseconds being relatively rare for this type of system. The longest/largest simulation of a lipid that has been reported to date (Lindahl and Edholm, 2000) [51] extends these factors by an order of magnitude. However, certain simplifying approximations were necessary to enable this calculation. Even so, the scales for time and space are still small compared to the time and length scales for some important lipid membrane phenomena [24].

One area where molecular dynamics often falls short is in reproducing measured electrostatic potential between the hydrocarbon interior of a bilayer and the adjacent water region [45, 52]. This may be due to two major problems in molecular dynamics: polarizability, as a function of neighboring nonbounded atoms is ignored, and long range dipolar interactions must be truncated somehow. Even with these drawbacks the results produced by molecular dynamics method still show much promise and in fact, this is the only technique to yield microscopic level description of the membrane system retaining consistency with thermodynamic and collective behavior [53].

## 1.5 OBJECTIVES AND OUTLINE

The objective of this study was to use molecular dynamic techniques to investigate physical properties of the hydrated DPPC bilayer at high pressures and temperatures. When available a comparison with the results of previous simulation and experimental works was also performed. An $L_\alpha$ phase bilayer was created during the initial system construction and simulation was performed at 1 atm pressure and 323 K temperature conditions in order to study the $L_\alpha$ phase. In addition to this, simulations were performed at high pressure (1000 atm and 2000 atm) and temperature (423 K) conditions to determine whether this method can be used to study high pressure and high temperature phases without complex equilibration procedures.

In Chapter 2 of this thesis; basic statistical mechanics concepts used to perform molecular dynamics simulations, methods used to parameterize the energy hypersurface, the Ewald summation method for long-range electrostatistic energy calculation, and Nose-Hoover methods used for NVT and NPT simulations will be presented. Initial bilayer construction, parameterization and simulation conditions will be given in Chapter 3. Results of the simulations will be discussed in Chapter 4. Summary of this study and further work will be given in Chapter 5.

# Chapter 2

# THEORY

## 2.1 MOLECULAR MECHANICS

### 2.1.1. Ensembles

Computer simulation produces information at the microscopic level (atomic and molecular positions, velocities etc.) and converts this very detailed information into macroscopic terms (pressure, internal energy etc.). This process is a part of statistical mechanics. Molecular dynamics simulations have been carried out under different microscopic boundary conditions. These conditions in a simulation can be treated in different ways. Boundary conditions are defined by a small set of parameters such as number of particles $N$, energy $E$, chemical potential $\mu$, temperature $T$, total volume $V$, and pressure $P$. There are several options in selecting a boundary condition: Micro-canonical ensemble ($E$, $V$ and $N$ constant), Canonical or NVT ($N$, $V$ and $T$ constant), Grand canonical ($T$, $V$ and $\mu$ constant) and isothermal–isobaric ensemble or NPT ($N$, $P$ and $T$ constant) [54]. Either NPT or NVT boundary conditions have been used in most studies. The size of a simulation box in NVT simulations is determined by using an experimental value for the area per lipid and the repeat distance for a given number of water molecules

or by using the total density. Under this condition, pressure of the system fluctuates during the simulation. In NPT simulations, box sizes fluctuate (length x, width y and height z independently of each other, or x and y coupled and z independent) in order to keep the pressure approximately constant. In addition, this process sometimes allows the box angles to fluctuate with the change of box size, abandoning a rectangular shape [55].

### 2.1.2 Phase–space

Phase-space trajectories are most often used to describe the molecular system in the simulation. The state of a classical system, at any instant in time, can be completely described by specifying the position $r$ and momenta $p$ of all particles. If the system has $N$ number of particles and the space is three dimensional, definition of a microstate requires the specification of $3N$ position coordinates $r_1, r_2, r_3, \ldots r_{3N} = \{r\}$ and $3N$ momentum coordinates $p_1, p_2, p_3, \ldots p_{3N} = \{p\}$. This $6N$ dimensional space is called phase-space or $\Gamma$-space. In this space, the total number of degrees of freedom is $6N - 6$. The phase point $(r_i, p_i)$ refers to a representative point for the system. The system of particles is described by the Hamiltonian $H$:

$$H = \sum_{i=1}^{N} \frac{p_i}{2m_i} + U \qquad 2.1$$

where $U$ is potential energy. The change in coordinates $r_i$ and momenta $p_i$ with time $t$ is determined by Hamilton's equations shown below [56].

$$\dot{r}_i = \frac{\partial H(r_i, p_i)}{\partial p^N} \qquad 2.2$$

$$\dot{p}_i = -\frac{\partial H(r_i, p_i)}{\partial r_i} \qquad 2.3$$

where $i = 1,2,3\ldots N$ and $H\{r, p\}$ is the Hamiltonian of the system.

## 2.1.3 Thermodynamic Averages

Thermodynamic properties of a system such as kinetic energy, volume, and pressure are functions of the coordinates and momenta of the particles in that system. These properties (averages) are independent of time in a state of equilibrium. Averages of these thermodynamic properties can be calculated in two ways: ensemble averages and time averages [54].

### 2.1.3.1 Ensemble Averages

Every member of the ensemble undergoes a continual change of microstates with time. Thus, the representative points continually move along their respective trajectories within the allowed region of the space.

The number of representative points around the point ($r_i$, $p_i$) of the phase-space is given by $\rho(r_i,p_i;t)\ d^{3N}r_i\ d^{3N}p_i$ at any time $t$. The $d^{3N}r_i\ d^{3N}p_i$ is the "volume element" and the $\rho(r_i,p_i;t)$ is the probability density function for the desired ensemble. The ensemble average $\langle f \rangle$ of a given physical quantity $f(r_i, p_i)$ can be given by [56]

$$\langle f \rangle = \frac{\int \ldots\ldots \int f(r_i, p_i)\rho(r_i, p_i; t) d^{3N} r_i d^{3N} p_i}{\int \ldots\ldots \int \rho(r_i, p_i; t) d^{3N} r_i d^{3N} p_i} \qquad 2.4$$

The ensemble average of any physical quantity $f$ must be independent of time if that ensemble is a stationary one.

### 2.1.3.2 Time Averages

The process of time averaging is completely independent from ensemble averaging. Here, $\langle f \rangle$ will be obtained by any member of the ensemble over long time period. $\langle f \rangle$ can be obtained as follows:

$$\langle f \rangle = \lim_{\tau \to \infty} \frac{1}{\tau} \int_0^{\tau} f[r_i(t), p_i(t)] \; dt \qquad 2.5$$

The equations of motion are usually solved step-by-step on a computer. Time length for one step is $\delta t = T/M$. T is the total time of simulation runs and M is the number of time steps. In this case, Equation 2.4 has to be rewritten in the form

$$\langle f \rangle = \frac{1}{M} \sum_{n=1}^{M} f[r_i(n), p_i(n)] \qquad 2.6$$

For more accuracy, this average has to be taken over the number of particles for a long time period [7].

## 2.2 FORCE FIELDS

A potential energy function along with a specified set of parameters is often referred to as a force field. Molecular dynamics simulations are based on force fields that govern all the relevant intramolecular and intermolecular energetic, structural and dynamics properties. Ranges of applicability and the accuracies of force fields have been limited by the way in which they were derived [57, 58]. Factors that affect the accuracy of molecular simulations include the treatment of solvent, counterions, and other species that may be present in the modeled environment, as well as other details of the simulation techniques.

### 2.2.1 Potential Energy Function

The potential energy is expressed as a sum of valence or bonded and non-bonded interactions. The valence interactions consist of bond, bond angle, and dihedral angle, terms. The non-bonded interactions consist of van der Waals terms and electrostatic terms. Bonds and angles are usually described as harmonic oscillators while dihedral angles are described by a suitable cosine expansion [59, 60, 61, 62]. The basic potential energy function is shown in Equation 2.7.

$$U(\vec{R}) = \sum_{\text{bonds}} K_b (b - b_0)^2 + \sum_{\text{angles}} K_\theta (\theta - \theta_0)^2 + \sum_{\text{dihedrals}} \frac{K_\phi}{2}[1 + \cos(n\phi - \gamma)] \qquad 2.7$$

$$+ \sum_{i<j} \varepsilon \left[ \frac{A_{ij}}{R_{ij}^{12}} - \frac{B_{ij}}{R_{ij}^{6}} \right] + \sum_{i<j} \frac{q_i q_j}{\varepsilon_0 r_{ij}}$$

where

| | |
|---|---|
| $b, \theta, \phi$ | - bond length, bond angles, and dihedral angle |
| $r_0, \theta_0, \phi_0$ | - equilibrium values for the individual terms |
| $K_r, K_\theta, K_\phi$ | - force constants for bonds, bond angles, and dihedral angle |
| $\varepsilon, R_{ij}$ | - Lennard-Jones well depth and distance at the Lennard-Jones minimum |
| $q_i, q_j$ | - partial charges for atom *i* and *j* |
| $r_{ij}$ | - distance between atom *i* and *j* |
| $A_{ij}, B_{ij}$ | - Lennard-Jones parameters |

Schematic expressions of bond length, bond angle, and dihedral angle are shown in Figure 2.1.

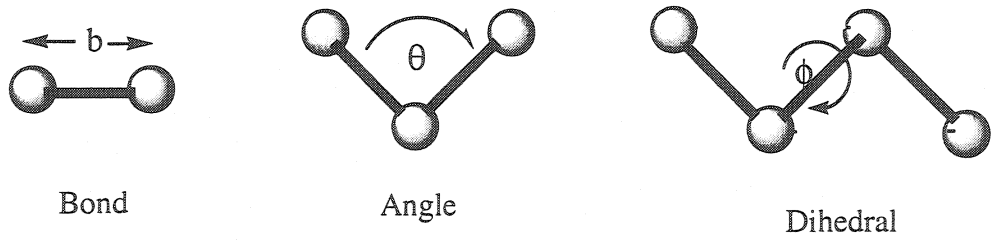


Figure 2.1: Schematic expressions of bond length, bond angle, and dihedral angle

In addition to bond, angle, dihedral angle, electrostatistic, and van der Waals interaction terms, some other terms may also be included in order to make the potential energy function more accurate. A hydrogen bond interaction term has been added to the potential energy function used in AMBER force field [10]. The improper dihedral angle term and the Urey-Bradley term have been included in CHARMM22 force field [63].

### 2.2.2 Parameterization

In order to obtain values for force field parameters, the potential energy function must be fitted to the experimental data from molecular mechanics calculations, theoretical data or some combination of both. The Consistent Force Field (CFF) is an example of the category where experimentally derived thermodynamic data (e.g. heats of formation) have been used to create the force field [63]. However, a lack of such experimental data, especially for large organic compounds or for coordination complexes, has often made it difficult and in some cases impossible to parameterize and test accurate force fields. It may become necessary to use *ab initio* data in the parameterization process when relevant experimental data is not available. Force fields such as CFF91 and Merck Molecular Force Field-93 (MMFF93) are parameterized using molecular properties determined by *ab initio* quantum chemical methods [64].

Force fields such as Assisted Model Building with Energy Refinement (AMBER) [10] and Chemistry at Harvard Macromolecular Mechanics (CHARMM) [11] are used in studying protein and nucleic acid macromolecules. Even though CHARMM was

originally devised for proteins and nucleic acids, it has now been applied to other biomolecules. Its usage has been extended to slow solvation, crystal packing and vibrational analysis problems [11].

The "united atom model" was commonly used for bilayer simulations in the 1980s and early 1990s [65]. In this method, alkyl groups in a particular molecule are treated as single "atoms" in order to reduce the number of atoms constituting the molecular system. This was performed to reduce the complexity of the intermolecular energy calculation, which must be performed at each integration time step. Treating a single DPPC molecule in this way reduces the number of atoms from 130 to 50, corresponding to a reduction in degrees of freedom from 780 to 300 [66]. However, force fields employed in the united atom model have been found to give incorrect hydrocarbon chain packing in bilayer simulations for example, due to an increase in collective chain tilt and low molecular volumes. At high pressure, according to experimental evidence, the hydrocarbon chains of lipid molecules may become interdigitated [21]. Increasing pressure has also been shown to result in a decreasing area per lipid [20]. Thus, there will exist a low free volume in the region of interdigitation and a detailed description of the chain structure may be important. Due to these facts, an "all atom force field" was thought to be necessary for high pressure simulations [66]. All atom force fields available today for studying organic systems include CHARMM22 [63], AMBER/OPLS [10], CFF93/95 [64], and COMPASS [67].

## 2.3 BOUNDARIES AND LONG RANGE FORCES

### 2.3.1 Periodic Boundary Conditions

Even with the availability of supercomputers, methods such as Monte Carlo and molecular dynamics can still only be applied to samples of relatively small number of particles, usually of the order of a few hundreds to a few thousands. The simulation system of that small size would leave too many molecules near the surface. Surface effects would dominate and the system would represent a cluster rather than a liquid in a liquid structure [68]. One way of avoiding these cluster artifacts is the use of periodic boundary conditions. In this approach, the simulation system consists of repetitions of the base unit in all directions. Only the base unit needs to be kept in the simulation as all the other units are related to the base unit by translational symmetry [68]. The potential energy per particle for a system interacting through a central force type potential due to the periodic conditions is given by

$$V = \frac{1}{N}\sum_{n}\sum_{j<i} U\left(r_{ij} + Ln\right) \qquad 2.8$$

where $N$ is number of particles in the box and $L$ is the length of a side. The summation is to be taken over all the molecule pairs within the simulation model. This method does not cause a problem for short-range interaction forces. However, this method introduces errors for long-range forces such as charge-charge interaction between ions as this equation converges only conditionally for long-range forces. Moreover, periodic

boundary conditions should be used only when the system is truly or nearly periodic. However, since periodic boundary conditions provide important advantages in a simulation, various correction schemes have been proposed in order to take the long-range forces into account.

### 2.3.2 Cut-offs and Long Range Forces

Both van der Waals interactions (proportional to $1/R^6$) and Coulomb interactions (proportional to $1/R$) decrease with the increase of distance. In general, these interactions are neglected after certain distance which is referred to as the 'cut-off point'. The cut-off procedure works best for van der Waals interactions. There are problems with using it for the Coulomb interactions. There is now a sizable amount of evidence that suggest that the cut-off method should be discontinued. However, it is still regularly employed in simulations.

The Ewald sum method is a better way to handle Coulombic interactions in molecular dynamics and Monte Carlo simulations employing periodic boundary conditions. This procedure was originally used to calculate the electrostatic interactions in crystals but it is ideal for charges of systems with infinitely repeating units like polymers and lipid bilayers. Ewald sum method cannot be used for non-periodic systems such as gas phase systems [69]. This method reduces the cost of calculating the Coulomb potential sum. The coulomb potential sum is split into two parts, one of which is

calculated directly or in real space, and the other is calculated in Fourier or reciprocal space [70]. The real space potential part is given by

$$E_{real} = \frac{1}{2}\sum_{i=1}^{N}\sum_{j=1}^{N}\left(\sum_{|n|=0}^{\infty}\frac{q_i q_j}{4\pi\varepsilon|r_{ij}+n|}erfc\left(\alpha|r_{ij}+n|\right)\right) \qquad 2.9$$

where $q_i$ and $q_j$ are charges of $i^{th}$ and $j^{th}$ particles and $r_{ij}$ is nearest-image antiparticles. First double summations are taken over all atoms. A third summation, over $n$, represents a sum over lattice vectors in three dimensions. '*erfc*' is the complementary error function (equation 2.10)

$$erfc(x) = 1 - \frac{2}{\sqrt{\pi}}\int_0^x e^{-t^2}dt \qquad 2.10$$

and the convergence parameter $\alpha$ is set so that $E_{real}$ is negligible after cutoff radius $r_{cut}$. Therefore, this term needs to be evaluated over only the nonbonded pairs of atoms with $n=0$. The reciprocal space part, given by,

$$E_{reciprocal} = \frac{1}{2\pi V}\sum_{i=1}^{N}\sum_{j=1}^{N}\sum_{k\neq 0}\frac{q_i q_j}{4\pi\varepsilon}\left(\frac{4\pi^2}{k^2}\right)\exp\left(\frac{-k^2}{4\alpha^2}\right)\exp\left(ik.r_{ij}\right) \qquad 2.11$$

where $V = L^3$ is the unit cell volume and k is the reciprocal lattice vector. The summation over $\mathrm{k} = 2\pi\left(\frac{l}{L_x},\frac{m}{L_y},\frac{n}{L_z}\right)$ represents a sum over reciprocal lattice vectors in three dimensions. In fully flexible box constant pressure simulations, a general definition for the k vector is [69],

$$k = 2\pi\left(h^{-1}\right)^{t}\begin{pmatrix} l \\ m \\ n \end{pmatrix} \qquad 2.12$$

where $h$ is box size tensor. In addition to the above two terms, the following two correction terms have been added to the total electrostatistic expression,

$$E_{self} = \frac{\alpha}{\sqrt{\pi}}\sum_{i=1}^{N}\frac{q_i^{\,2}}{4\pi\varepsilon} \qquad 2.13$$

$$E_{excl} = \sum_{i=1}^{N}\sum_{j\in N_i^{excl}}\frac{q_i q_j erfc\left(\alpha\left|r_i - r_j\right|\right)}{4\pi\varepsilon\ \left|r_i - r_j\right|}. \qquad 2.14$$

$E_{self}$ cancels the interaction of the charges with themselves. $E_{excl}$ cancels charge distribution between an atom and atoms in its excluded atom list in molecular systems.

The total electrostatic interaction is calculated by equation 2.15

$$E_{total} = E_{real} + E_{reciprocal} - E_{self} - E_{excl}. \qquad 2.15$$

## 2.4 NOSE-HOOVER CHAIN (NHC) METHODS

### 2.4.1 Constant Temperature Molecular Dynamics (NVT)

Most experimental measurements are performed at constant temperature rather than constant energy. Therefore, temperature control is an essential step in molecular dynamics simulation. Many methods have been developed in order to control temperature of a simulation. Crude [71] introduced a method to maintain the system

temperature $(T_d)$ at a constant value by scaling the velocities of the particles at each time step or every several time steps by a factor of $(T_d/T_r)^{1/2}$. $T_r$ is the calculated temperature of the system. Brendan *et al.* [72] modified the method by scaling the velocity by a factor of $\left[1+\frac{dt}{r_T}\left(\frac{T_d}{T_r}-1\right)\right]^{1/2}$, where $dt$ is the time step and $r_T$ is the temperature coupling constant. This method is very efficient in equilibrating to a new temperature but does not correspond to any existing ensemble.

Nose [73, 74, 75] introduced an extended system method by coupling the system to a heat bath. He derived a dynamics from of an extended Hamiltonian that can be shown to give canonically distributed positions and momenta. In this method, an extra degree of freedom associated with the heat bath is included. Martyna *et al.* [76] modified the equations of motion by introducing a chain of thermostats and formed a Nose-Hoover chain (NHC) algorithm.

The set of dynamical equations in NHC algorithm [76],

$$\dot{r}_i = \frac{p_i}{m_i} \qquad 2.16$$

$$\dot{p}_i = \frac{\partial V(r)}{\partial r_i} - p_i \frac{p_{\xi_1}}{Q_1} \qquad 2.17$$

$$\dot{\xi}_i = \frac{p_{\xi_i}}{Q_i} \qquad 2.18$$

$$\dot{p}_{\xi_1} = \left[\sum_{i=1}^{N} \frac{p_i^2}{m_i} - N_f kT\right] - p_{\xi_1} \frac{p_{\xi_2}}{Q_2} \qquad 2.19$$

$$\dot{p}_{\xi_j} = \left[\frac{p_{\xi_{j-1}}^2}{Q_{j-1}} - kT\right] - p_{\xi_j}\frac{p_{\xi\, j+1}}{Q_{j+1}} \qquad 2.20$$

$$\dot{p}_{\xi_M} = \left[\frac{p_{\xi_{M-1}}^2}{Q_{M-1}} - kT\right] \qquad 2.21$$

where r and p are the positions and momenta, $M$ is the number of thermostats on the chain, $\xi$ and $p_\xi$ are the thermostat variable and its conjugated momentum, $Q_i$ is the mass of the $i^{th}$ thermostat, $k$ is the Bolzmann constant, $N_f$ is the number of degrees of freedoms (for $N$ partials in d-dimensional system $N_f = Nd$). The extended Hamiltonian or conserved quantity can be express by following equation.

$$H'(p,r,p_\xi,\xi) = U(r) + \sum_{i=1}^{N}\frac{p_i^2}{2m_i} + \sum_{i=1}^{M}\frac{P_{\xi_i}^2}{2Q_i} + NkT\xi_1 + \sum_{i=2}^{M}kT\xi_i \qquad 2.22$$

where U(r) is the total potential energy.

The phase space distribution for dynamics equations is

$$f(p,r,p_\xi,\xi) \propto \exp\left\{-\frac{1}{kT}\left[U(q) + \sum_{i=1}^{N}\frac{p_i^2}{2m_i}\right] + \sum_{i=1}^{M}\frac{p_{\xi_i}^2}{2Q_i}\right\}. \qquad 2.23$$

## 2.4.2 Constant Pressure Molecular Dynamics (NPT)

The same amount of attention has been directed to the development of constant pressure algorithms. Berenden *et al.* [72] developed a method to keep pressure constant. They introduced a scaling factor μ,

$$\mu = \left[1 - \beta_T \frac{dt}{t_P}(P_d - P_r)\right]^{1/3} \qquad 2.24$$

where $dt$ is time step, $\beta_T$ is the isothermal compressibility, $P_r$ is the calculated instantaneous pressure, and $t_p$ is noncritical time constant. The coordinates of the particles and the simulation box are scaled by $\mu$ to keep pressure of the system $P_d$ constant. Parrinelo and Rahman [77] have also developed a method to keep the system pressure constant by allowing both the volume and shape of the simulation box to vary freely.

Martyna *et al.* [78] introduced Nose-Hoover (NHC) chain algorithm to form isobaric- isothermal simulations. This NHC algorithm allows changing the size and the shape of the box.

$$\dot{r}_i = \frac{p_i}{m_i} + \frac{\tilde{p}_g}{W_g} r_i \qquad 2.25$$

$$\dot{p}_i = F_i - \frac{\tilde{p}_g}{W_g} p_i - \left(\frac{1}{N_f}\right)\frac{Tr\left[\tilde{p}_g\right]}{W_g} p_i - \frac{p_\xi}{Q} p_i \qquad 2.26$$

$$\dot{\vec{h}} = \frac{\vec{p}_g \vec{h}}{W_g} \tag{2.27}$$

$$\dot{\vec{p}}_g = V(\vec{P}_{\text{int}} - \vec{I}P_{ext}) + \left[\frac{1}{N_f}\sum_{i=1}^{N}\frac{p_i^2}{m_i}\right]\vec{I} - \frac{p_\xi}{Q}\vec{p}_g \tag{2.28}$$

$$\dot{\xi} = \frac{p_\xi}{Q} \tag{2.29}$$

$$\dot{p}_\xi = \sum_{i=1}^{N}\frac{p_i^2}{m_i} + \frac{1}{W_g}Tr\left[\vec{p}_g^{\,t}\vec{p}_g\right] - (N_f + d^2)kT \tag{2.30}$$

where $h$ and $p_g$ are the box dimension tensor and the conjugated momentum. $W_g$ is the barostat mass, $p_g$ is the barostat momentum, $P_{ext}$ is the external pressure, $V = \det\left[\vec{h}\right]$, I is identity matrix, $Tr\left[\vec{p}_g^{\,t}\vec{p}_g\right]$ is the sum of the squares of all the elements of the matrix $p_g$, and $P_{int}$ is internal pressure. Thus,

$$\left(P_{\text{int}}\right)_{\alpha\beta} = \frac{1}{V}\left[\sum\left(\frac{(p_i)_\alpha (p_i)_\beta}{m_i} + (F_i)_\alpha (r_i)_\beta\right) - \left(\vec{U}'\vec{h}^{\,t}\right)_{\alpha\beta}\right] \tag{2.31}$$

where $\vec{U}' = \dfrac{\partial U\left(r,\vec{h}\right)}{\partial(h)_{\alpha\beta}}$

The extended Hamiltonian or conserved quantity for isothermal-isobaric dynamics is,

$$H' = U(r,\vec{h}) + \sum_{i=1}^{N}\frac{p_i^2}{2m_i} + \frac{p_\xi^2}{2Q} + \frac{1}{2W_g}Tr\left[\vec{p}_g^{\,t}\vec{p}_g\right] + P_{ext}\det\left[\vec{h}\right] + (N_f + d^2)kT\xi \tag{2.32}$$

The new dynamical equation leading to the partition function is

$$Z = \frac{\exp[E/kT]}{(N_f + d^2)kT} \int dp_\xi d\vec{h} dp_g \int_{D(\vec{h})} dpdr \det\left[\vec{h}\right]^{1-d} \exp\left[-\frac{H''}{kT}\right] \qquad 2.33$$

where $H'' = U(r,\vec{h}) + \sum_{i=1}^{N} \frac{p_i^2}{2m_i} + \frac{p_\xi^2}{2Q} + \frac{1}{2W_g} Tr\left[\vec{p}_g^{\,t}\, \vec{p}_g\right] + P_{ext} \det\left[\vec{h}\right]$

Different groups have applied the Nose-Hoover Chain method (NHC) to solve a large number of complex problems. Cheng and Merz [79] used NHC for protein dynamics and Deng *et al.* [80] used NHC methods in quantum studies of metal-ammonia solutions. NHC method is also used in ROAR program in NVT and NPT simulations [69].

# Chapter 3

# SIMULATION METHODOLOGY

## 3.1 INITIAL CONSTRUCTION OF THE DPPC BILAYER

X-ray crystallographic data for DMPC molecules at $L_c$ phase [17] was used in constructing the initial structure for a DPPC molecule. Using this data, a Protein Databank (PDB) file was created by using the Crystal Builder module of the Cerius$^2$ 2.0 program [81]. Two additional alkyl groups were added to both acyl chains in a trans conformation in DMPC molecule in order to make the DPPC molecule (Figure 3.1) and then the atoms were assigned names and CHARMM22 partial charges and force field atom types with the help of the AMBER LEaP program. Five thousand minimization steps were performed on the DPPC molecule by using the ROAR program. This was performed to ensure that the bond lengths in the DPPC molecules matched the CHARMM22 parameters closely.

The initial bilayer was constructed from the DPPC molecules generated as mentioned above. This bilayer consists of 25 DPPC molecules per each monolayer. The area per lipid was set to 68.1 Å$^2$, which is the experimental data for a bilayer system with a water percentage by weight of about 45% [82]. Five hundred steps of energy

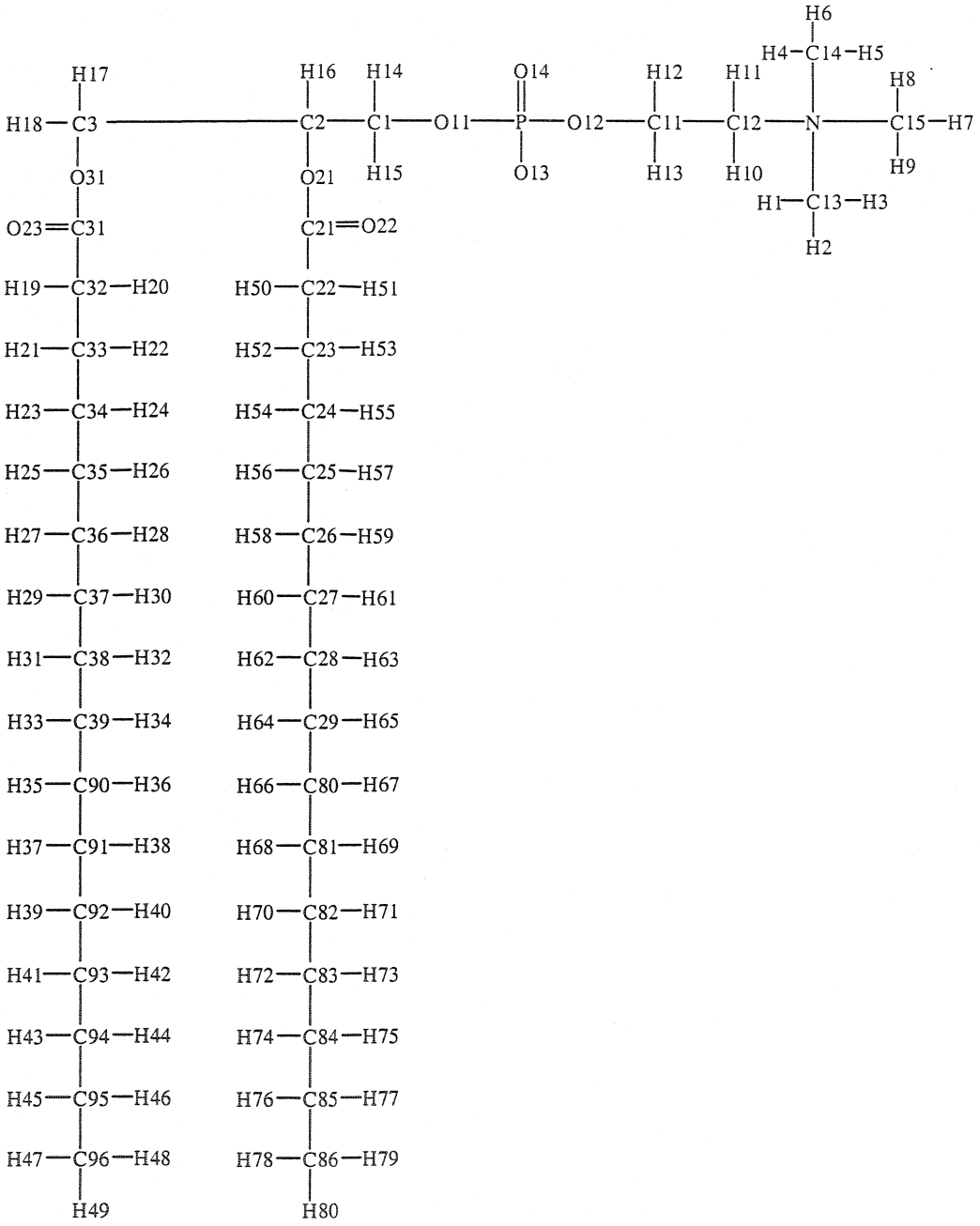


Figure 3.1 Atomic names for DPPC

minimization were performed on the system to remove close contacts. Water molecules in the TIP3P model of Jorgensen *et al.* (1983) [83] were added as a 15 Å thick layer on both sides of the bilayer using a modified version of the AMBER EDIT program. The total number of water molecules in the system is 1656. This gave 33.12 water molecules per lipid molecule or 44.8% water by total weight of the bilayer system. Finally, 500 energy minimization steps were performed on the total system to remove remaining bad contacts among the atoms.

## 3.2 FORCE FIELD PARAMETERIZATION

A modified version of the CHARMM22 force field for phospholipids is used in this study. As previously mentioned (Section 2.2.2), the potential function used in CHARMM22 includes all atoms explicitly [63]. The energy function (Equation 3.1) contains two additional terms other than the terms include in the basic potential energy function (Equation 2.7): improper dihedral angle ($\varphi$) and Urey-Bradley bond length ($S$) shown in Figure 3.2.

$$U(\vec{R}) = \sum_{\text{bonds}} K_b (b - b_0)^2 + \sum_{UB} K_{UB} (S - S_0)^2 + \sum_{\text{angles}} K_\theta (\theta - \theta_0)^2$$

$$+ \sum_{improper} K_{imp} (\varphi - \varphi_0)^2 + \sum_{\text{dihedrals}} \frac{K_\phi}{2} [1 + \cos(n\phi - \gamma)] \qquad 3.1$$

$$+ \sum_{i<j} \left[ \frac{A_{ij}}{R_{ij}^{12}} - \frac{B_{ij}}{R_{ij}^{6}} \right] + \sum_{i<j} \frac{q_i q_j}{\varepsilon r_{ij}}$$

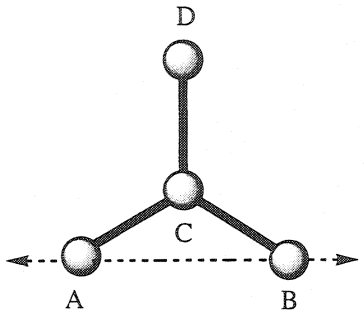


(a) Improper Torsion

( The improper angle φ is defined as the angle between the planes *ABC* and *BCD* )

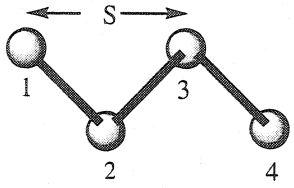


(b) Urey-Bradley 1,3 distance

Figure 3.2 CHARMM22 improper angle and Urey-Bradley bond length

The improper dihedral angle (Figure 3.2a) has been introduced to keep the CCOO structure in phospholipids (Figure 1.3) planar [66]. The Urey-Bradley bond length (Figure 3.2b) is the distance between atoms 1 and 3. This term is introduced when the bond angle term is thought to be insufficient to accurately reproduce the interaction energy between three bonded atoms.

In this version of CHARMM, initial values of the intermolecular parameters (Coulomb and Lennard-Jones) have been chosen based on the reproduction of *ab initio* interaction calculations on small monomers [63]. Given these values, the intramolecular parameters (bond length, Urey-Bradley, bond angle, dihedral angle, and improper dihedral angle terms) have been determined by using structural and vibrational data for the model compounds [63]. The resulting structures were then used for optimization of the intermolecular parameters relative to interaction energies and condensed-phase properties of model compounds. The interaction parameters (partial atomic charges and

Lennard-Jones parameters) have been optimized based on *ab initio* results for water/model compound interactions and from macroscopic thermodynamic properties calculated via Monte Carlo simulations [84].

## 3.3 MOLECULAR DYNAMICS SOFTWARE

AMBER software was used in this study as it has most of the features required for this work and also due to its relatively low cost. This is a well-known molecular dynamics software that can be used in simulating biomolecules. AMBER programs include components useful in the construction of initial system configurations, simulation of these systems, and analysis of the simulation results [10]. The code allows some variation in functional form as well as parameters of the force field. These variations include alternate functions for improper torsions and Urey-Bradley interactions. Therefore, CHARMM22 force fields can be used with AMBER energy programs such as SANDER and ROAR [10].

The molecular dynamics energy program ROAR1.0 [69] that is included in AMBER5.0 [10] was used in performing molecular dynamics simulations and energy minimization in the present study. *LEaP*, which is another program included in AMBER5.0, was used in preparing initial input for the ROAR1.0. The Nose-Hoover Chain algorithms [76] are combined with an explicit reversible integrator [85] in ROAR1.0 in order to solve Newton's equations of motion and to control the temperature and pressure during a simulation. The Ewald sum method with spherical cutoff was used in calculating long-range electrostatic interactions [7].

When using the ROAR1.0 program, simulations can be performed under NVT or NTP conditions [69]. Under NTP conditions, the ROAR software eliminates bond vibrations with the SHAKE/RATTLE method [86]. In the SHAKE algorithm, a guess is made as to what constraint forces would be required to maintain constant bond lengths. On the other hand, the RATTLE algorithm is used to ensure there is a zero net velocity along the bond length between two bonded atoms. A 15% increase in cpu time required for one time step has been observed for NPT simulations where the RATTLE and SHAKE procedures were used [69]. The SHAKE/RATTLE constrain was used in this study since the vibrational modes of pairs of bonded atoms will not be examined.

## 3.4 SIMULATION CONDITIONS

The all atom CHARMM22 force field was used to parameterize lipids with 12 Å spherical cutoff. The TIP3P water model was used to hydrate the system. Each molecule in the system was treated as a group. Cutoff of 12 Å was used for longer-range interactions. The SHAKE tolerance of 0.0005 Å was used to constrain bond lengths. The isothermal-isobaric or NPT ensemble with a fully flexible simulation box was used as microscopic boundary conditions for this study because it is particularly useful for membranes. This ensemble allows validating simulations by checking their ability to reproduce important structural parameters such as the area per lipid and bilayer thickness when they are known, and to predict these parameters when they are unknown. These simulations were run under different pressure (1 atm, 1000 atm and 2000 atm) and temperature (323 K, 423 K) conditions in order to study the change in physical

parameters of the bilayer system under different temperature-pressure combinations. All simulations were run for 1.5 – 2.0 ns time period with 1 fs time steps. Area per lipid, bilayer thickness, chain tilt, and total energy of the system at different pressure temperature combinations were analyzed.

Simulations were carried out on eight SGI Onyx 3400, 400 MHz processors; sixteen SGI Origin model 2400, 400 MHz processors; and sixteen SGI Origin model 3800, 400 MHz processors. Eight 400 MHz processors took 336 cpu hours (42 Clock time hours) to reach ~90 ps time period and sixty 400 MHz processors took 376 cpu hours (23.5 Clock time hours) to reach ~75 ps time period.

# Chapter 4

# RESULTS AND DISCUSSION

## 4.1 SIMULATION AT 1 ATMOSPHERIC PRESSURE AND 323 K TEMPERATURE

Simulation at 1 atm pressure and 323 K temperature conditions was performed up to 2 ns time period in order to study physical properties of the bilayer such as area per lipid, bilayer thickness, chain tilt, and order parameters. Initially, the integration time step for the modified Nose-Hoover Chain equations was set to 1 fs. The thermostat and barostat masses are important in determining the rate at which atomic velocities and positions are rescaled in order to maintain constant temperature and pressure. Therefore proper choices of the thermostat and barostat masses are essential to reach equilibrium. When very small masses are chosen, bond length and velocities may fluctuate rapidly leading to constraint algorithm failure. In this study, thermostat and barostat masses changed to 12 and 1.2 respectively from the default values (1.0 and 0.3) of ROAR program after performing several simulations with different values. Without these changes, the SHAKE/RATTLE algorithms were found to fail after a short period of time. The reciprocal lattice vector was set to 6 while the real cutoff was set to 12 Å. These values were determined by increasing the real and reciprocal space cutoffs alternatively until the electrostatic energy was approximately converged.

Figure 4.1 shows how H´ changed with time during the simulation. According to Nose-Hoover Chain method, the H´ should be a conserved quantity. However, Figure 4.1 indicates that H´ increased proportionally with time in this simulation.

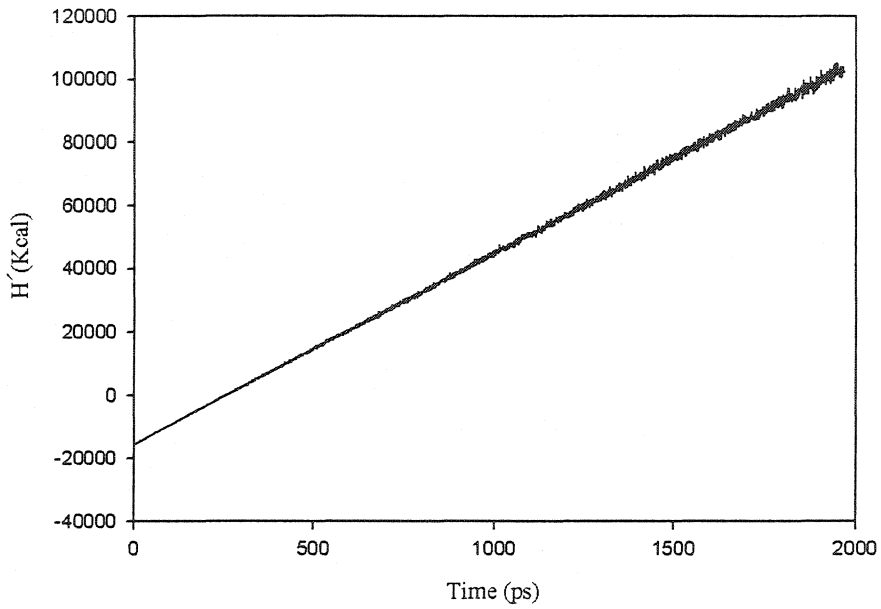


Figure 4.1: H´ as a function of time for the DPPC bilayer simulation at 323 K temperature and 1 atm pressure

When we consider Equation 2.32, the sum of the first two terms is constant (Figure 4.3) and the third and fourth terms of the equation have very small contribution to the H´ value. Fifth term is the PV term and that is again a constant. Thus, the increase in H´ is due to the term involving the thermostat (see Figure 4.2). The $\left(N_f + d^2\right)kT\xi$ term is the potential energy related to the thermostat position $\xi$ (Equation 2.32). In this term, factors $\left(N_f + d^2\right)$, k, and T are constant. Thus, it is the increase in thermostat position, $\xi$, that causes the increase in H´. The thermostat variable controlled the system

temperature well during the simulation (Figure 4.4). However, it might have been necessary to supply heat by thermostat in order to control system temperature as the system itself is cooling down with simulation time. This might have led to the increase in H′.

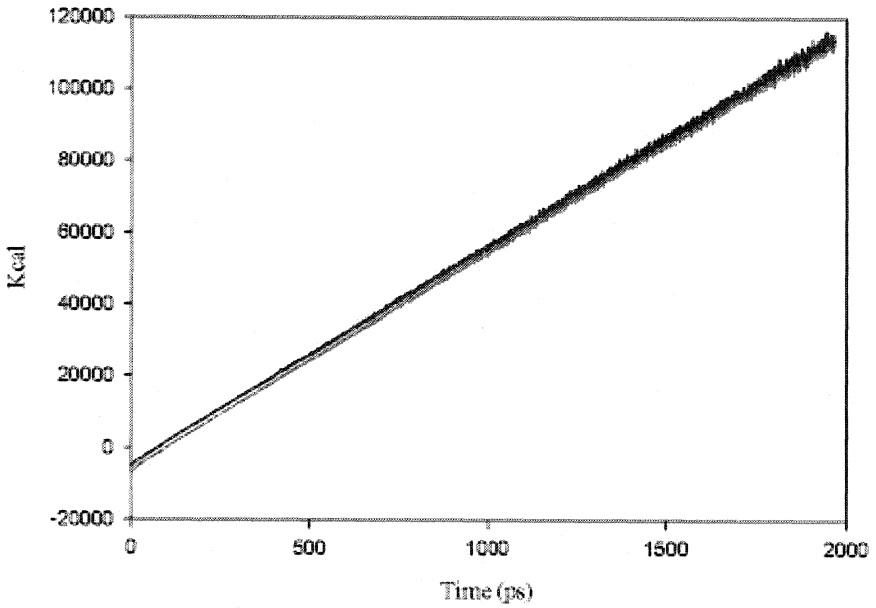


Figure 4.2: $\left(N_f + d^2\right)kT\xi$ term (Black) with H′ (Red) as a function of time for the DPPC bilayer simulation at 323 K temperature and 1 atm pressure

The bilayer system should be equilibrated in order to interpret results produced from a simulation. However, the examination of properties calculated before equilibration may still provide information about the equilibrium state of the system. For example, if the bulk quantities (i.e., quantities which depend on large number of molecules such as area per lipid and bilayer thickness) are converging to a reasonable value, one can conclude that the system has reached an equilibrium. Further, according

to Figure 4.3, the total system energy had converged within a 1000 ps time period. Thus, the physical properties of the bilayer such as area per lipid, bilayer thickness, chain tilt, and order parameters were evaluated after 1000 ps.

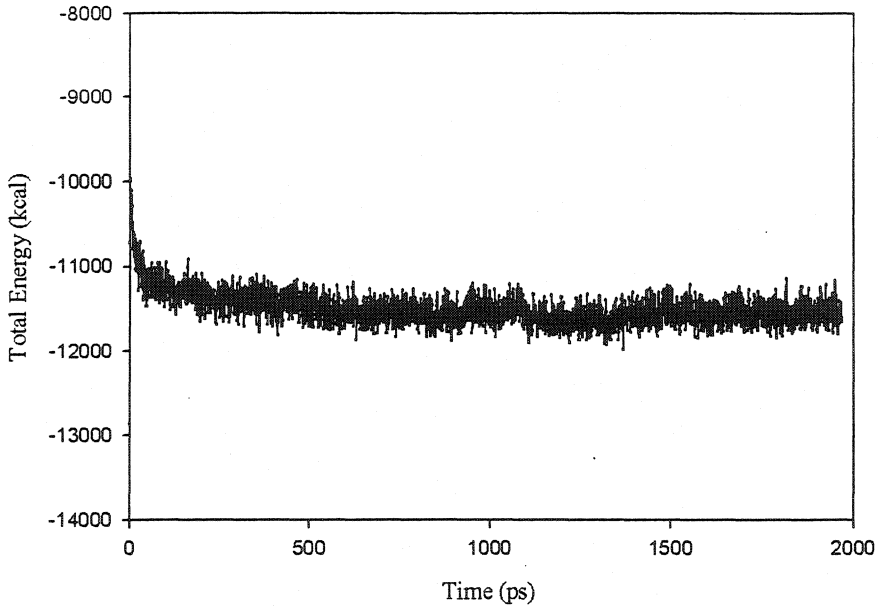


Figure 4.3: Internal energy as a function of time for the DPPC bilayer simulation at 323 K and 1 atm

The variation of system temperature and pressure in the simulation are shown in Figure 4.4 and Figure 4.5a respectively. The system temperature varied slightly around 323 K and was controlled reasonably by the Nose-Hoover Chain algorithms used in this study. However, the pressure variation was considerably high. In addition, the average value of system pressure was slightly higher than 1 atm. X, Y and Z components of system pressure as a function of time for the DPPC bilayer simulation at 323 K and 1 atm are shown in Figure 4.5b. These figures show that the system pressure applied in this simulation was nearly isotropic.

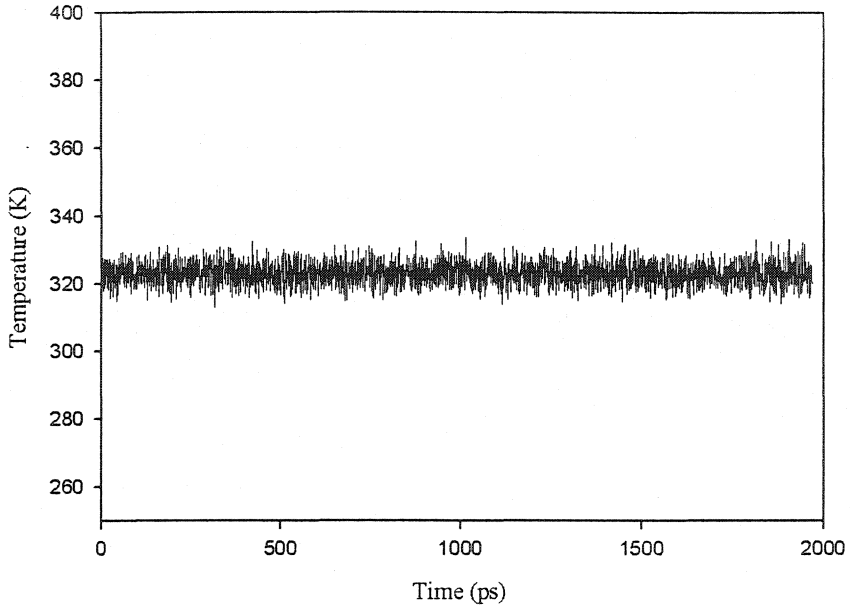


Figure 4.4: System temperature as a function of time for the DPPC bilayer simulation at 323 K and 1 atm.

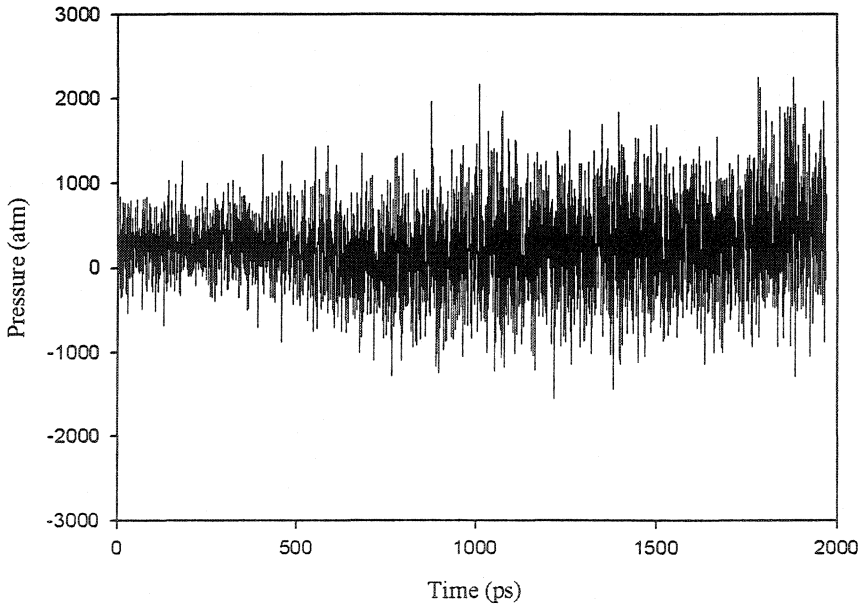


Figure 4.5a: System pressure as a function of time for the DPPC bilayer simulation at 323 K and 1 atm.

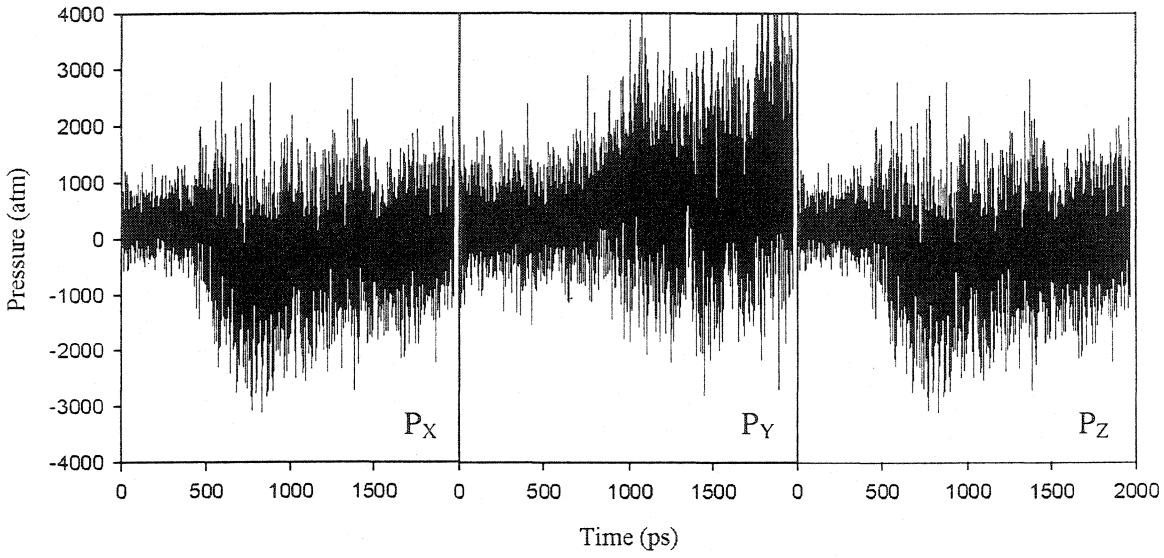


Figure 4.5b: X, Y and Z components of system pressure as a function of time for the DPPC bilayer simulation at 323 K and 1 atm.

### 4.1.1 Area Per Lipid

The average area per DPPC head group can be used as a convenient measure of molecular packing in the DPPC bilayer. The periodic boundary conditions used in this work allow the surface planes of the bilayer (defined as the planes formed by the head group phosphorus atoms) to be parallel to the plane containing the lattice vectors $\bar{a}$ and $\bar{c}$ (Appendix E). The cross sectional area per lipid may then be calculated according to the following formula:

$$A = \frac{1}{25} \parallel \bar{a} \times \bar{c} \parallel$$

where 25 is the number of lipids in one monolayer. Figure 4.6 illustrates the time evolution of the surface area per lipid along with the experimental $L_\alpha$ and $L_{\beta'}$ values from references [92] and [91], respectively. According to Figure 4.6, the area per lipid converged within 1000 ps, after which it fluctuated around a certain value with a small amplitude. This result also indicates the system equilibration within 1000 ps. The average value for area per lipid was hence calculated for the last 1000 ps time period. This value is 48.85 ± 0.44 Å$^2$ and is represented by the solid horizontal line in Figure 4.6.

In literature, structural data has been obtained using various experimental methods. For $L_\alpha$ phase of the DPPC bilayer, area per lipid values reported are 71.2 Å$^2$ [89], 68 Å$^2$ [90] (by gravimetric X-ray (GX) method), 68.1 Å$^2$ (by corrected gravimetric (GXC) method) [91], and 62.9 Å$^2$ (by electron density profile (EDP) method) [92]. For the $L_{\beta'}$ phase, the experimental values according to literature are 52.3 Å$^2$ [89], 50 Å$^2$ [90], 48.6 Å$^2$ [88] (by GX method), 48.6 Å$^2$ (by GXC method) [91], and 47.9 Å$^2$ (by EDP method) [93]. There is a scatter in experimental results possibly due to uncertainties in obtaining structural results by using methods mentioned above.

According to phase diagrams of Figure 1.6 [17] and Figure 1.9 [23], a liquid crystal phase ($L_\alpha$) was expected for the present DPPC bilayer simulated under 1 atm pressure and 323 K temperature conditions. Instead, a gel-like phase ($L_{\beta'}$) was observed when comparing with the previous experimental data mentioned above for the area per lipid of the DPPC bilayer. In fact, the average area per lipid value (48.85 ± 0.44 Å$^2$) is very close to the experimental results reported for $L_{\beta'}$ phase [88, 91, 93].

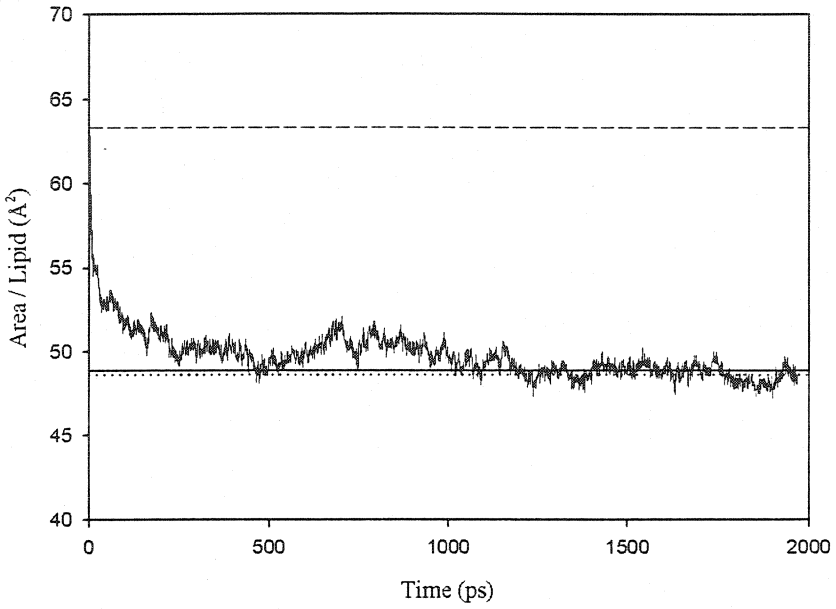


Figure 4.6: Time evolution of the area per DPPC molecule during the constant NPT simulation of the DPPC bilayer at 323 K and 1 atm. The solid line represents the average value for area per lipid calculated for the last 1000 ps. Dashed line and dotted line represent the experimental values for $L_\alpha$ [92] and $L_{\beta'}$ [91] phases respectively.

### 4.1.2 Bilayer Thickness

The thickness of a bilayer in X-ray diffraction studies is determined as the distance between the two peaks of maximum electron density, which occurs on the phosphate anion regions of the polar head groups [94]. In order to be consistent with diffraction data the bilayer thickness in molecular dynamics simulations is taken as the distance between the two planes which best fit the phosphorus atom position in the upper and lower monolayers. Bilayer thickness as a function of time is shown in Figure 4.7 along with experimental $L_\alpha$ and $L_{\beta'}$ values from reference [89].

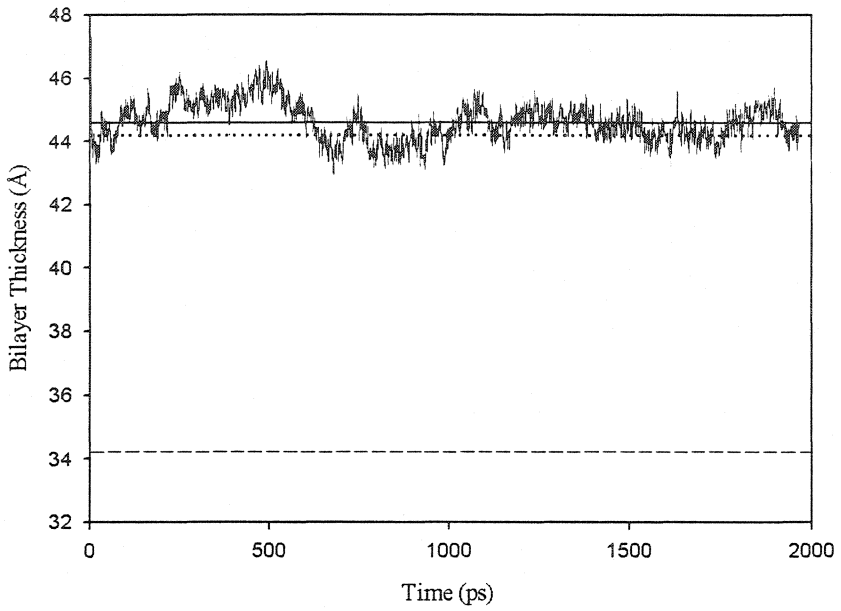


Figure 4.7: Time evolution of the DPPC bilayer thickness during the constant NPT simulation at 323 K and 1 atm. The solid line represents the average value for thickness calculated for the last 1000 ps. Dashed line and dotted line represent the experimental values for $L_\alpha$ and $L_{\beta'}$ phases respectively [89].

The average value of bilayer thickness for the last 1000 ps period is 44.57 ± 0.33 Å. Experimental values of DPPC bilayer thickness according to Lis *et al.* (1982) [89] are 34.2 Å for $L_\alpha$ phase and 44.2 Å $L_{\beta'}$ phase. Thus, similarly to the area per lipid results, the present bilayer thickness at 1 atm and 323 K is close to the experimental value of $L_{\beta'}$ phase.

### 4.1.3 Average Chain Tilt

The angle of chain tilt is defined as

$$\theta_{tilt} = \frac{\vec{r}_{ch} . \hat{n}}{\| \vec{r}_{ch} \|}$$

where vector $\vec{r}_{ch}$ is the vector connecting a carbon atom near the tail of a hydrocarbon chain and a carbon atom near the beginning of the chain, and $\hat{n}$ is the unit vector of the bilayer normal direction. In this study, the vector $\vec{r}_{ch}$ has been taken by averaging the vector from carbon C85 (95) to C23 (33) (Figure 3.1) over all chains in a monolayer.

Figure 4.8 shows how the average chain tilts of monolayers vary with the time in this simulation. The horizontal solid line and the dashed line represent the average values for the bottom monolayer (33.67° ± 1.25°) and the top monolayer (28.03° ± 1.10°) respectively. Dotted horizontal line represents the experimental value of chain tilt for DPPC bilayer in $L_{\beta'}$ phase. The simulated average tilt values of the present study remain close to experimental value (29.78 °) [95] of $L_{\beta'}$ phase.

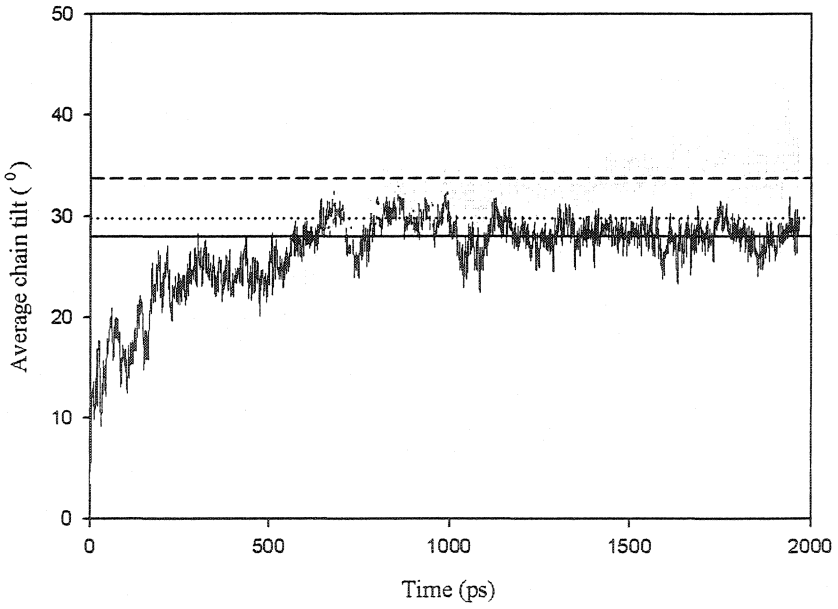


Figure 4.8: Time evolution of the average chain tilt at 323 K and 1 atm: top monolayer (black), bottom monolayer (gray). Average values for the average chain tilt values represent by horizontal lines: top monolayer (solid line), bottom monolayer (dashed line), and experimental value for $L_{\beta'}$ phase (dotted line).

### 4.1.4 Order Parameters

The disorder in acyl chains can be most effectively represented by the molecular order parameter profile. The order parameter of $j^{th}$ alkyl group in a lipid hydrocarbon chain is defined as

$$S_{CD} = \frac{1}{2}\left\langle 3\cos^2\theta_j - 1 \right\rangle$$

where $\theta_j$ is the angle between the bilayer normal to the plane formed by the carbon atom and the two hydrogen atoms bonded to it. The averaging is done over all alkyl groups in the bilayer which have the same chain position. Order parameters obtained in this study are shown in Figure 4.9.

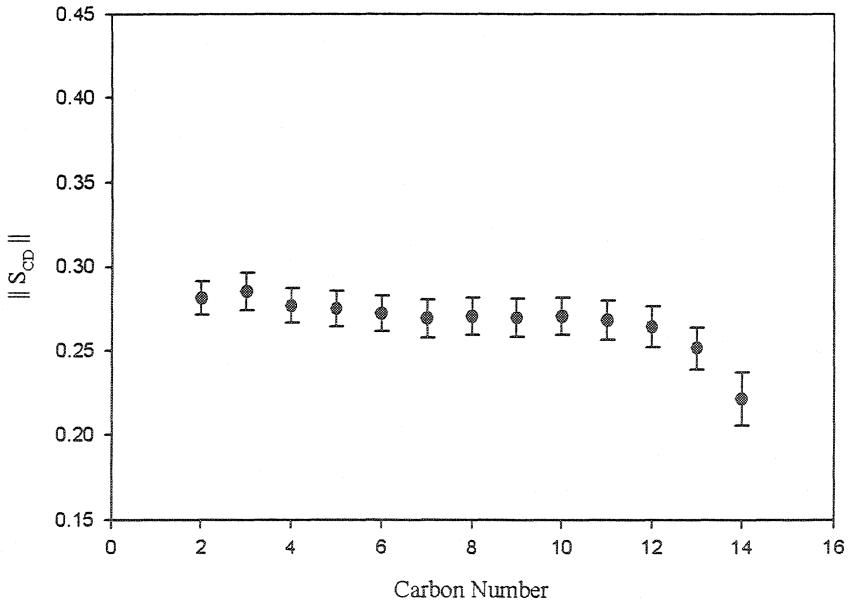


Figure 4.9: Order parameters as a function of carbon atom numbers at 323 K and 1 atm.

Orientational order parameter profiles for DPPC at 1 atm pressure and and 348 K temperature have been reported by Driscoll *et al.* (1991) [96]. The values reported for $L_\alpha$ phase DPPC bilayer according to them were all less than about 0.2. In another study of DPPC order parameter profiles [97], the plateau values of order parameters for liquid crystalline DPPC were also around 0.2. Experimental values for $S_{mol}$, which is twice the $S_{CD}$, for $L_{\beta'}$ phase of DPPC-water system have been found to be between 0.2 to 0.3 [98]. Order parameter results from the present study varied between 0.2 – 0.3, that were higher than the results obtained from the studies mentioned above. Data for the gel phase is more difficult to find from experiments due to the fact that order parameters cannot be as easily extracted from gel phase deuterium NMR spectra as from corresponding liquid crystal spectra.

As discussed above, physical properties obtained by the simulation of the DPPC bilayer system with 46 % water by weight at 1 atm pressure and 323 K temperature conditions indicate an existence of a gel like phase ($L_{\beta'}$). At this temperature, pressure, and water content an $L_\alpha$ phase should be observed [17, 23]. The initial system construction consisted of phospholipid with their acyl chains in an all *trans* conformation, with the area per lipid equal to 68.1 $Å^2$ which is consistent with an $L_\alpha$ phase bilayer. As shown in Figure 4.10, this initial construction was followed by a rapid increase in system density which fluctuated around a constant value afterwards. One explanation for this may be the expulsion of water molecules from the bilayer system constructed. Graphical representations of the initial bilayer and the bilayer system after 2 ns simulation at 323 K and 1 atm are shown in Appendices E and F respectively.

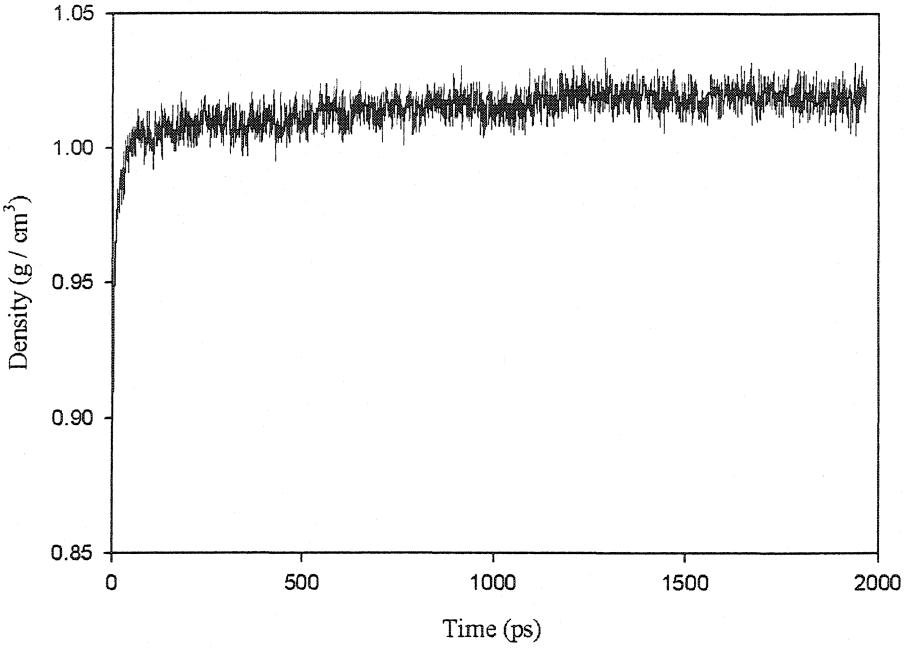


Figure 4.10: Time evolution of the density.

The CHARMM22 force field used in this study has been noted for giving too high densities in simulations [66]. A possible explanation as to why an $L_{\beta'}$ phase bilayer is forming may be that flaws in the force field are being augmented by the particular equations of motion used in this study. However, an NPT simulation conducted by Shinoda *et al.* (1997) [99] using an OPLS/AMBER force field with 32 DPPC and 434 water molecules (TIP4P model) under periodic boundary condition at 353 K and 1 atm (i.e., $L_{\alpha}$ phase) has also reported similar area per lipid and order parameters results as obtained in the present study (Figures 4.6 and 4.9). They have also reported area per lipid (53.9 Å$^2$) and order parameter values (between 0.1 – 0.25) that are close to

experimental values of $L_{\beta'}$ phase. NPAT (where A is the area per lipid) simulation conducted by Venable and Pastor (1997) [30] has used CHARMM program with PARM22b4b parameter set for their study along with a lipid bilayer of 72 DPPC molecules and approximately 2000 water molecules. The simulation performed at 1 atm and 323 K with different constant area per lipids (59.3, 62.9, 65.5, or 68.1 $Å^2$) had resulted in different chain tilt and order parameter values depending on the initial area per lipid used. Moreover, even at 68.1 $Å^2$/lipid, their chain tilt is close to the average chain tilt value as obtained in this study.

## 4.2 SIMULATION AT 1 ATMOSPHERIC PRESSURE AND 423 K TEMPERATURE

In section 4.1 we showed that, even though an $L_\alpha$ phase should result, physical properties obtained by the simulation of the DPPC bilayer system with 45 % water by weight at 1 atm pressure and 323 K temperature conditions resulted in a gel like phase ($L_{\beta'}$). Thus, it was decided to increase the system temperature up to 423 K (by keeping other simulation conditions such as molecular dynamics parameters, initial system, and pressure similar to the simulation performed at 323 K) in order to study how the resultant bilayer properties would change accordingly. This simulation study was performed up to 600 ps and the same physical parameters discussed in Section 4.1 were evaluated under these conditions. Graphical representation of the bilayer system after 600 ps simulation at 423 K and 1 atm are shown in Appendix G. The variation of H′, system temperature and pressure in this simulation (see Appendix B) showed a similar pattern to that of at 323 K (Section 4.1).

According to previous experimental studies, when the temperature or hydration of the bilayer system increased further, the $L_{\beta'}$ phase undergoes a phase transition first to the $P_{\beta'}$ or $P_{\beta}$ phase and then to the liquid crystal ($L_{\alpha}$) phase (Figure 1.6) [17].

### 4.2.1 Area Per Lipid

According to Figure 4.11, area per lipid after 600 ps had not converged completely. However, when compared to the average area per lipid value at 323 K (48.85 ± 0.44 Å$^2$, Figure 4.6), an increase in area per lipid could be observed at 423 K (53.61 ± 0.49 Å$^2$, by taking average for last 100 ps) (Figure 4.11). These results are closer to experimental results of $L_{\alpha}$ phase than the results obtained at 1 atm pressure and 323 K temperature conditions in this study (Section 4.1).

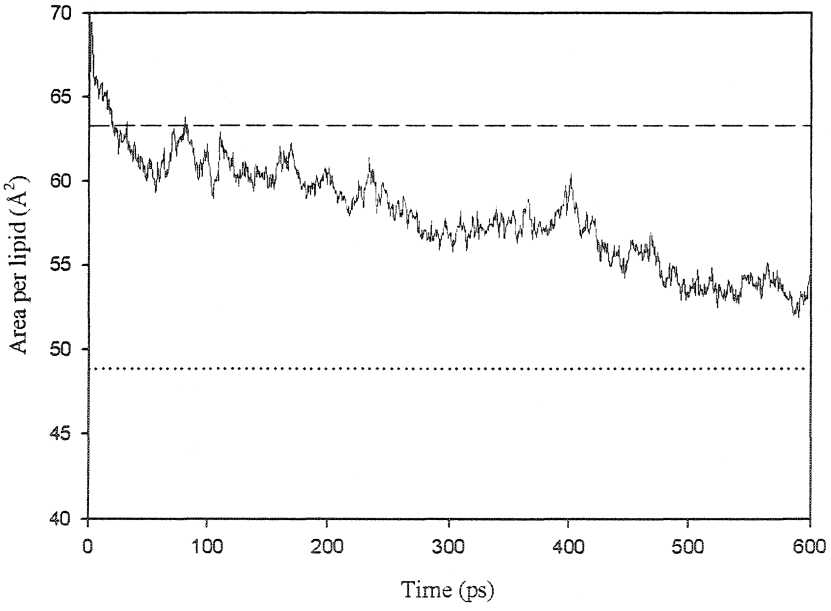


Figure 4.11: Time evolution of the area per DPPC molecule during the constant NPT simulation of the DPPC bilayer at 423 K and 1 atm. Dashed line and dotted line represent the experimental values for $L_{\alpha}$ [92] and $L_{\beta'}$ [91] phases respectively.

### 4.2.2 Bilayer Thickness

Bilayer thickness at 423 K after 600 ps (Figure 4.12) is close to the experimental value of $L_{\beta'}$ phase [89] similar to the simulation result obtained at 323 K. However, high variability could be observed in bilayer thickness with a lower starting value compared to the simulation at 323 K (~ 44 Å).

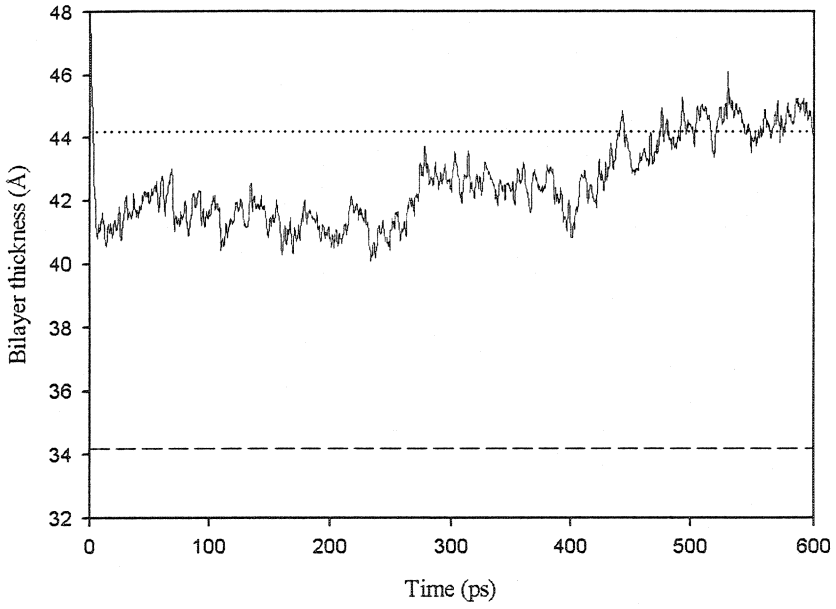


Figure 4.12: Time evolution of the DPPC bilayer thickness during the constant NPT simulation at 423 K and 1 atm. Dashed line and dotted line represent the experimental values for $L_{\alpha}$ and $L_{\beta'}$ phases respectively [89].

### 4.2.3 Average Chain Tilt

Average chain tilt values at 423 K varied between 0 – 25 ° (Figure 4.13) and are lower than at 323 K [the bottom monolayer (33.67° ± 1.25°) and the top monolayer

(28.03° ± 1.10°) respectively, Section 4.1.3]. Further, average chain tilt values at 423 K are lower than the experimental value for the $L_{\beta'}$ phase (29.78 °) [95].

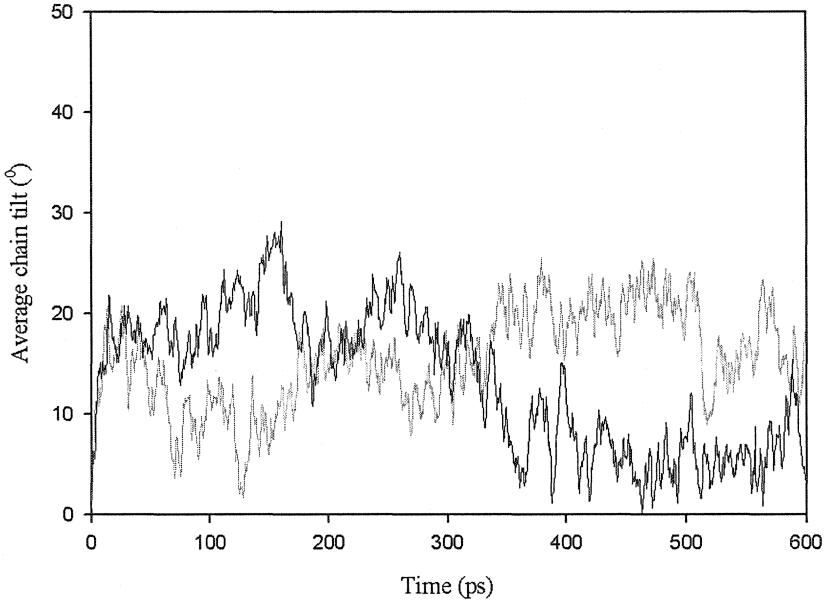


Figure 4.13: Time evolution of the average chain tilt at 423 K and 1 atm: top monolayer (black), bottom monolayer (gray).

## 4.2.4 Order Parameters

Order parameters obtained at 423 K and 1 atm in this study are shown in Figure 4.14. Order parameter variation is larger when comparing with the values obtained at 323 K temperature (Figure 4.9). At 323 K, order parameters of C2 – C10 carbon atoms remained close to ~0.27 and showed a slight decrease at the end of the alkyl chain (~ 0.22 for C14). Similarly, at 423 K, there was a plateau region between C3 and C10 where $S_{CD}$

was ~0.28, but showed lower order (~0.17) (Figure 4.14) at the end of the chains compared to the order for C13 and C14 at 323 K (Figure 4.9).

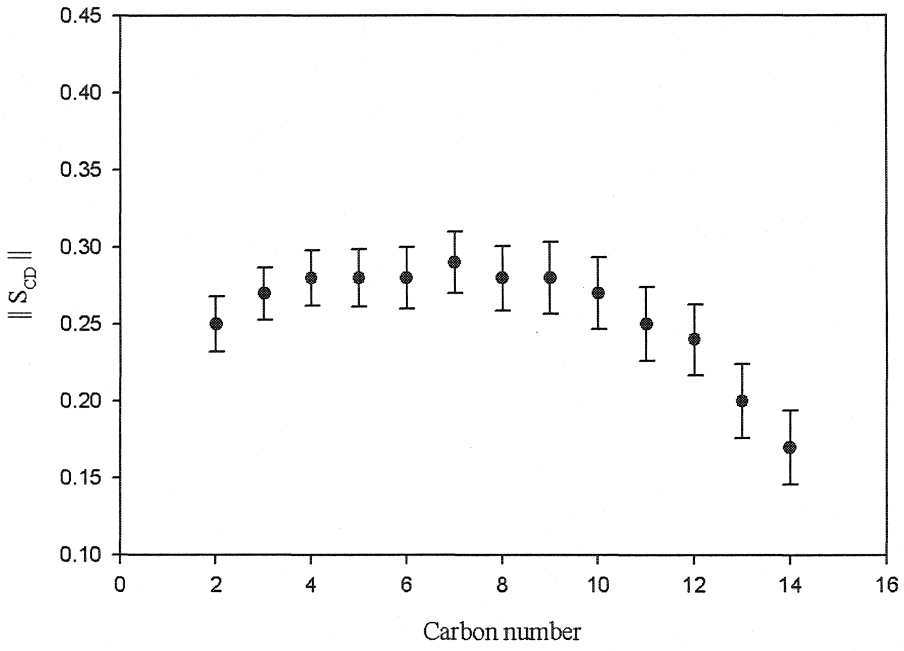


Figure 4.14: Order parameters as a function of carbon atom numbers at 423 K and 1 atm

According to Feller *et al.* (1997) [100], increase in temperature of the DPPC bilayer system may increase disorder by lowering $S_{CD}$ values for carbon atoms. However, this phenomenon could only be observed in a significant amount for C13 and C14 carbon atoms in this study.

## 4.3 SIMULATION AT 1000 ATMOSPHERES PRESSURE AND 323 K TEMPERATURE

Bilayer system pressure was increased to 1000 atm by keeping other simulation conditions such as molecular dynamics parameters, initial system, and system temperature constant as described in Section 4.1. This simulation study was performed up to 1.5 ns to study how the changes in physical parameters take place with the increase of system pressure. Graphical representation of the bilayer system after 1.5 ns simulation at 323 K and 1000 atm are shown in Appendix H. The same physical parameters discussed in Section 4.1 were evaluated under these conditions. According to Figure 1.9, DPPC bilayer with this pressure and temperature conditions should be in Gel I phase or $P_{\beta'}$ phase. However, experimental results for bilayer properties such as area per lipid, bilayer thickness for $P_{\beta'}$ phase could not be found from literature. This may be due to the difficulty in performing experiments at these extreme conditions. Thus, the results obtained from this simulation study at 1000 atm pressure will be compared with $L_{\alpha}$ and $L_{\beta'}$ phase experimental results. The variation of H′, system temperature and pressure in the simulation are shown in Appendix C.

### 4.3.1 Area Per Lipid

The average value for area per lipid of 46.55 ± 0.30 $Å^2$ is represented by the solid horizontal line in Figure 4.15. The area per lipid is smaller at 1000 atm than at 1 atm pressure (Figure 4.6). When comparing with experimental values, the average area per

lipid value under these conditions is even below the experimental $L_{\beta'}$ phase value. Thus, it can be predicted that the area per lipid decreases when the pressure of the system increases. Lis *et al.* [89] have also observed this phenomenon experimentally at constant temperature.

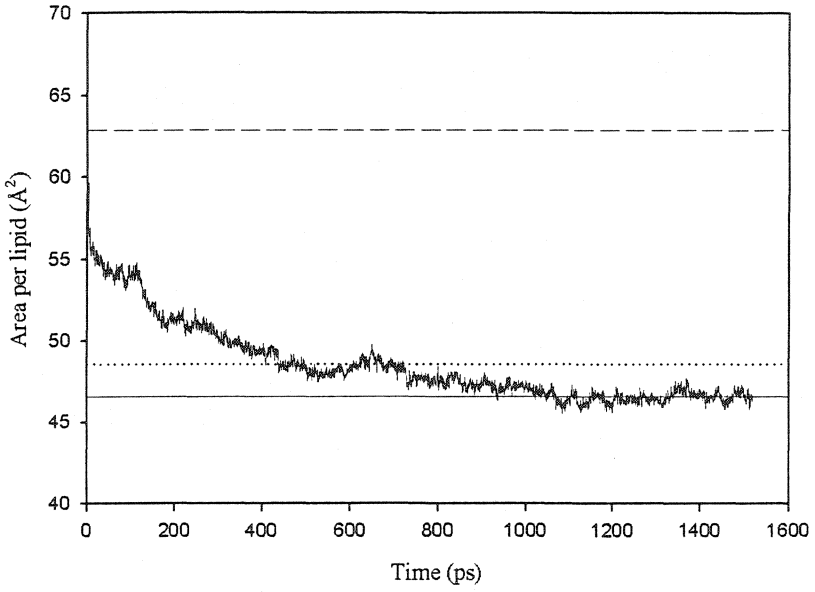


Figure 4.15: Time evolution of the area per DPPC molecule during the constant NPT simulation of the DPPC bilayer at 323 K and 1000 atm. The solid line represents the average value for area per lipid calculated for the last 600 ps. Dashed line and dotted line represent the experimental values for $L_{\alpha}$ [92] and $L_{\beta'}$ [91] phases respectively.

## 4.3.2 Bilayer Thickness

Figure 4.16 shows bilayer thickness variation with time. Average value of bilayer thickness is 46.02 ± 0.23 Å and represented by solid horizontal line. Bilayer thickness at 1000 atm pressure is greater than that of at 1 atm (Figure 4.7) and also than the

experimental value for $L_{\beta'}$ phase. The thickness variation may be inversely related to the variation of area per lipid and the bilayer can be assumed to be volumetrically incompressible.

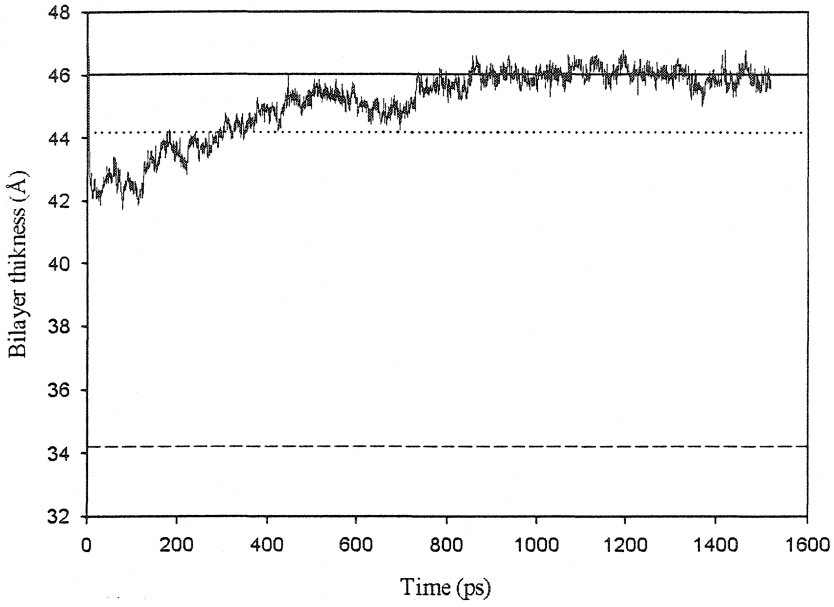


Figure 4.16: Time evolution of the DPPC bilayer thickness during the constant NPT simulation at 323 K and 1000 atm. The solid line represents the average value for thickness calculated for the last 600 ps. Dashed line and dotted line represent the experimental values for $L_{\alpha}$ and $L_{\beta'}$ phases respectively [89].

### 4.3.3 Average Chain Tilt

Both top and bottom monolayer chain tilt variation with time are shown by black and gray lines, respectively, in Figure 4.17. The top monolayer was still not converged completely with this time period while bottom monolayer tilt had converged to a value with a small variation around it. Solid and dashed lines show average values of chain tilt for top (8.42° ± 1.82°) and bottom (23.82° ± 1.34°) monolayers after 1000 ps. Both values had decreased when the pressure was increased to 1000 atm relative to bilayer at 1

atm pressure (Figure 4.8). It could be observed that when pressure increases, the area per lipid decrease and the chain tilt also decreased accordingly and came closer towards the bilayer normal.

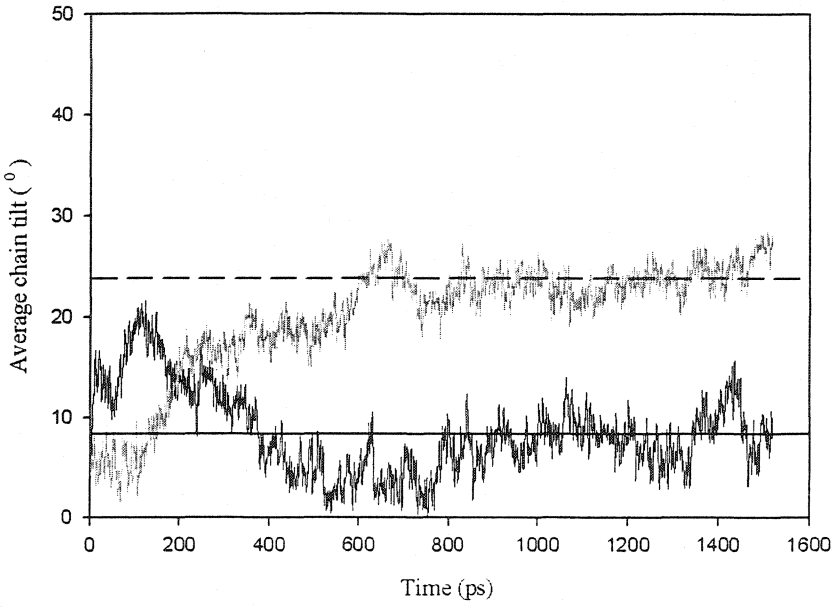


Figure 4.17: Time evolution of the average chain tilt at 323 K and 1000 atm: top monolayer (black), bottom monolayer (gray). Average values for the average chain tilt values represent by horizontal lines: top monolayer (solid line), bottom monolayer (dashed line).

### 4.3.4 Order Parameters

Order parameters obtained at 323 K and 1000 atm in this study are shown in Figure 4.18. Order parameter variation is larger when compared to the values obtained at 1 atm pressure. In addition to that, all values have increased with the increase of system pressure. This implies an increase in order of the system under this pressure and temperature condition. Experimental study performed by Driscoll *et al.* (1991) [96] had

also pointed out the fact that order parameter profiles increase with the increase of pressure from 1 atm – 1200 atm at 348 K.

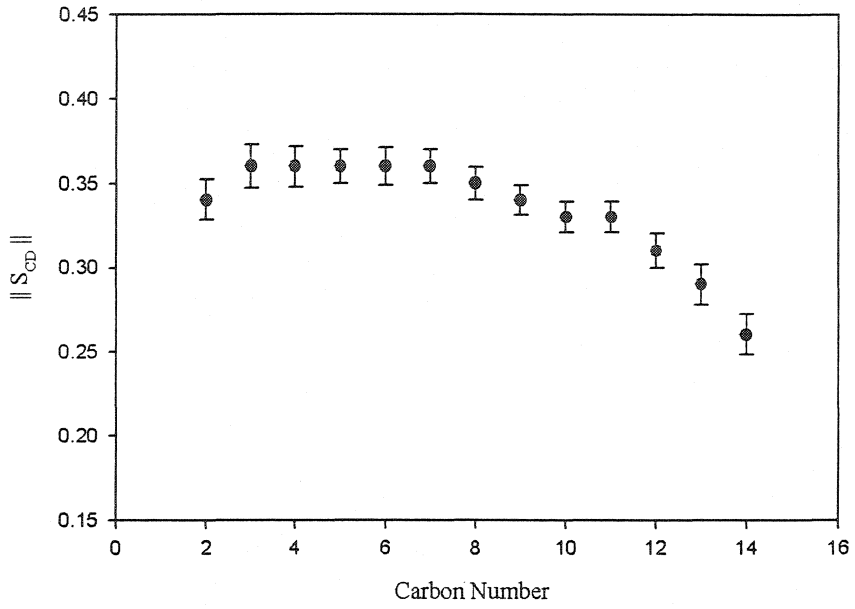


Figure 4.18: Order parameters as a function of carbon atom numbers at 323 K and 1000 atm.

## 4.4 SIMULATION AT 2000 ATMOSPHERES PRESSURE AND 323 K TEMPERATURE

Pressure was increased further up to 2000 atm in order to study physical properties of lipid bilayer at this high pressure. Temperature, initial system, and molecular dynamics parameters were kept the same as those described in Section 4.1 and the simulation was performed up to 1.7 ns. Graphical representation of the bilayer system after 1.7 ns simulation at 323 K and 2000 atm are shown in Appendix I. According to Figure 1.9, the DPPC bilayer at 2000 atm pressure and 323 K temperature should be in

the interdigitated phase. The variation of H′, system temperature and pressure in the simulation are shown in Appendix D.

### 4.4.1 Area per Lipid

Figure 4.19 illustrates how the area per lipid varied with time during the simulation. Area per lipid had converged with first 500 ps. When comparing with previous sections, this shows a rapid convergence. Thus, the physical properties of the bilayer such as area per lipid and bilayer thickness were evaluated after 500 ps. No significant differences could be observed for average area per lipid (46.55 ± 0.41 $Å^2$) result at 2000 atm compared to the result (46.55 ± 0.30 $Å^2$) obtained at 1000 atm.

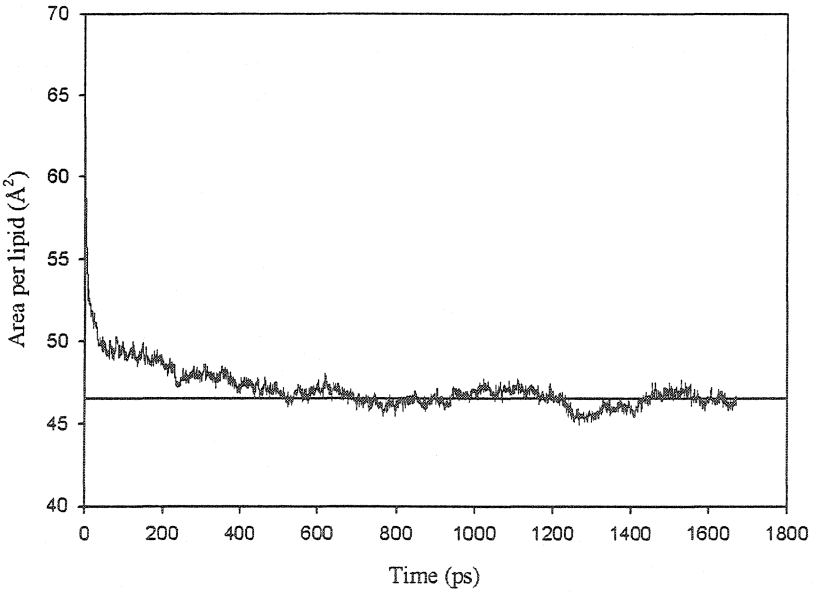


Figure 4.19: Time evolution of the area per DPPC molecule during the constant NPT simulation of the DPPC bilayer at 323 K and 2000 atm. The solid line represents the average value for area per lipid calculated for the last 1300 ps.

### 4.4.2 Bilayer Thickness

Similarly to the area per lipid under these conditions, bilayer thickness shows a rapid convergence (Figure 4.20). However bilayer thickness shows a higher variation around the average value than the variation of area per lipid (Figure 4.19). A slight decrease could be observed for average bilayer thickness (45.15 ± 0.35 Å) results at 2000 atm compared to the result (46.02 ± 0.23 Å) obtained at 1000 atm and is slightly higher than the one at 1 atm (44.57 ± 0.33 Å).

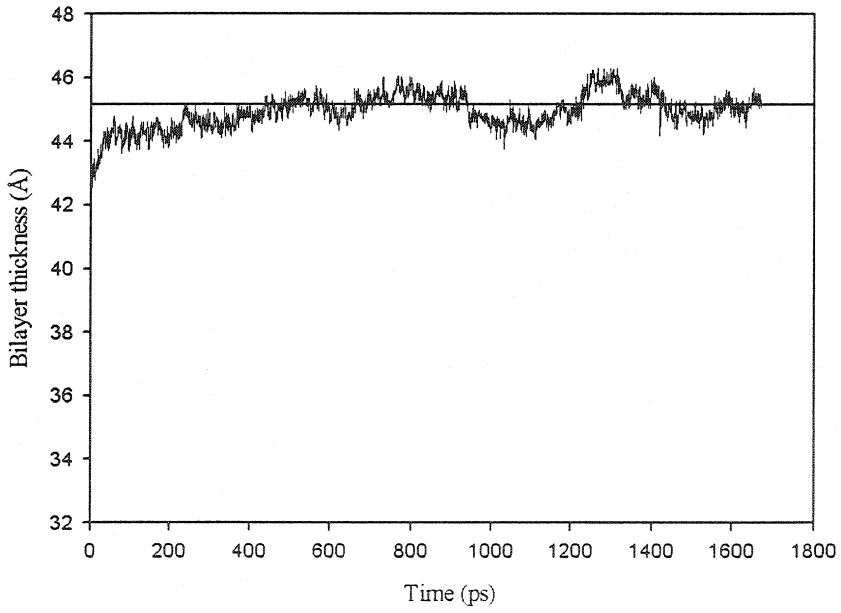


Figure 4.20: Time evolution of the DPPC bilayer thickness during the constant NPT simulation at 323 K and 1 atm. The solid line represents the average value for thickness calculated for the last 1300 ps.

### 4.4.3 Average Chain Tilt

The top and bottom monolayer chain tilts variation with time during the simulation are shown in Figure 4.21. Average chain tilt values for the top and bottom monolayers are very close and are 17.19° ± 1.32° and 18.68° ± 1.32° respectively (which were obtained after 1000 ps in the simulation). These values are less than chain tilt values at 1 atm pressure conditions (Figure 4.8).

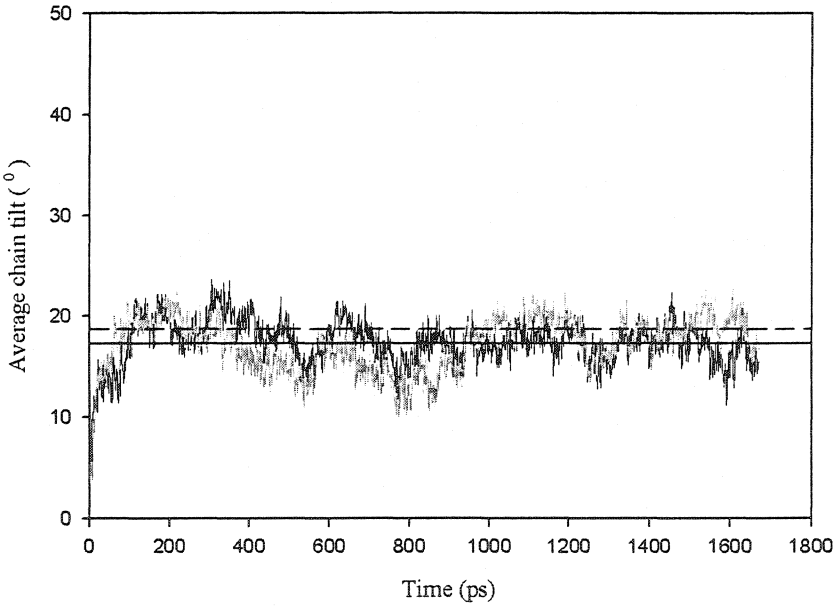


Figure 4.21: Time evolution of the average chain tilt at 323 K and 2000 atm: top monolayer (black), bottom monolayer (gray). Average values for the average chain tilt values represent by horizontal lines: top monolayer (solid line), bottom monolayer (dashed line).

### 4.4.4 Order Parameters

Both at 1000 and 2000 atm, order parameters for C2 to C8 carbon atoms are similar. But, the carbon atoms at the end of alkyl chains show higher order parameter values at 2000 atm (Figure 4.22) indicating greater ordering of chains at high pressure.

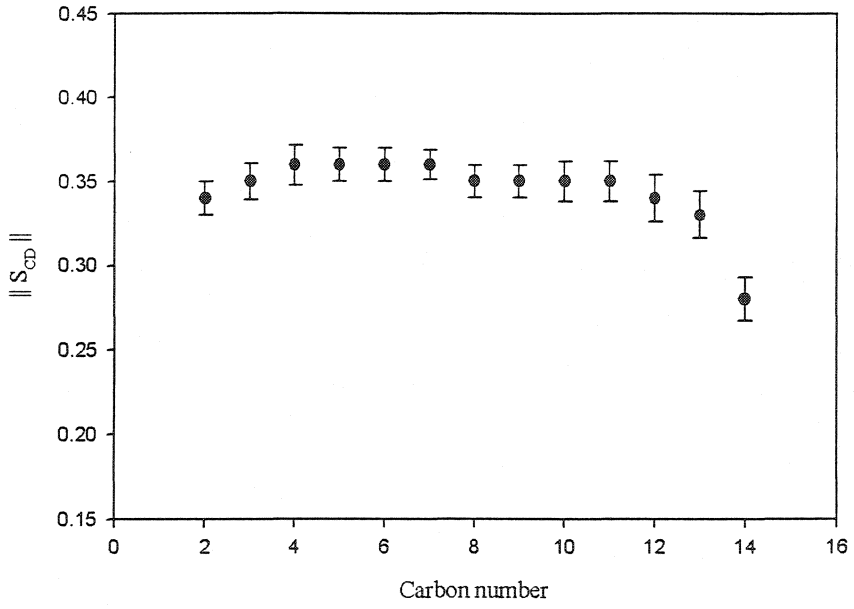


Figure 4.22: Order parameters as a function of carbon atom numbers at 323 K and 2000 atm.

# Chapter 5

# CONCLUDING REMARKS

## 5.1 SUMMARY OF RESULTS

Fifty DPPC molecules with 1656 water molecules (TIP3P model) were used to construct the initial bilayer system and the simulations were performed using ROAR molecular dynamic program. At 1 atm pressure and 323 K temperature, the equilibration phase of the simulation was completed at 1000 ps when the internal energy of the system had stabilized. Physical properties of the bilayer system such as area per lipid (48.85 ± 0.44 $Å^2$), bilayer thickness (44.57 ± 0.33 Å), chain tilt (the bottom monolayer: 33.67° ± 1.25° and the top monolayer: 28.03° ± 1.10°), and the order parameters (0.2 – 0.3) appears to be consistent with the experimental results of $L_{\beta'}$ phase under these conditions even though the desired equilibrium structure for the 1 atm simulation was that of an $L_\alpha$ phase bilayer.

An increase of temperature up to 423 K increased the area per lipid of the bilayer system. However, no significant difference could be seen between bilayer thickness values under 423 K and 323 K temperature conditions at 1 atm. Average chain tilt values at 423 K varied between 0 – 25 ° and were lower than at 323 K. Furthermore, end of alkyl chains showed more disorder at 423 K compared to at 323 K. Exact conclusion

could not be given at this point about the bilayer changes as the simulation at 423 K was performed only up to 600 ps and had not converged within this time.

| | Pressure (atm) at 323 K | | | | Experimental value | |
|---|---|---|---|---|---|---|
| | 1 | 1000 | 2000 | 1 atm & 423 K | $L_\alpha$ | $L_\beta$ |
| Area per lipid ($Å^2$) | 48.85 ± 0.44 | 46.55 ± 0.30 | 46.55 ± 0.41 | 53.61 ± 0.49 | 62.9 | 48.6 |
| Bilayer thickness (Å) | 44.57 ± 0.33 | 46.02 ± 0.23 | 45.15 ± 0.35 | 44.10 ± 0.48 | 34.2 | 44.2 |
| Average chain tilt top monolayer | 28.03° ± 1.10° | 8.42° ± 1.82° | 17.19° ± 1.32° | ~12° | - | 29.78° |
| Average chain tilt bottom monolayer | 33.67° ± 1.25° | 23.82° ± 1.34° | 18.68° ± 1.32° | ~12° | | |

Table 5.1: Summary of physical properties for different pressure and temperature combinations

Increase of system pressure up to 1000 atm at constant temperature (323 K) decreased the area per lipid while increasing the bilayer thickness compared to the results obtained at 1 atm. Further increase of pressure up to 2000 atm did not change the area per lipid significantly from 1000 atm and slightly decreased bilayer thickness. Average chain tilt values were considerably different for top and bottom monolayers at 1000 atm. However, at 2000 atm, both monolayers had similar average tilt values and greater ordering was observed. The results obtained in this study are summarized in Table 5.1 and Figure 5.1.

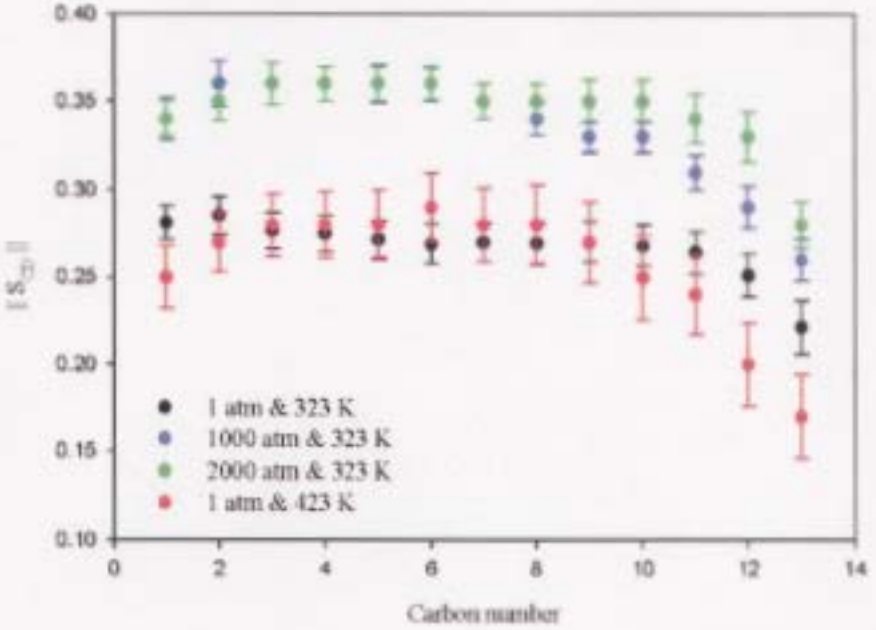


Figure 5.1: Order parameters as a function of carbon atom numbers at different pressure and temperature combinations

## 5.2 FURTHER WORK

The simulations in this study, like other molecular dynamic studies of membrane systems, is limited by the system size and time scale. More accurate physical results of the bilayer system would require extensive ensemble averaging by performing simulation for much longer time periods with supercomputers. Simulation at 423 K in the present study must be performed for a longer time period before final conclusions can be made.

One of the most important tasks in simulation is generating a suitable starting bilayer structure. In this study, the initial bilayer has been chosen from available experimental data, but there is considerable amount of uncertainty of these experimental results. As an example, for the DPPC bilayer at $L_\alpha$ phase, area per lipid results varies from 57 to 71.2 $Å^2$. On the other hand, considering the initial collapse of the bilayer

system, the simulation should be performed by changing initial physical properties of the system such as area per lipid which may lead to different final results. According to Figure 1.6, the initial bilayer system constructed in this study should create a bilayer of an $L_\alpha$ phase with some excess water in the system. This excess water may create problems in such a small bilayer system. Thus, it would be better to add only a sufficient amount of water to hydrate the system in order to create the desired phase at the desired temperature and pressure condition. United atom force field may be used for lipid bilayer systems with much less computational time. In this Nose-Hoover Chain method, velocities and positions depend on the adjustable parameters such as thermostat and barostat. Therefore, it may be useful to perform simulations by changing these parameters in order to obtain better results.

# REFERENCES


1. Haile, J.M. 1992. *Molecular Dynamics Simulation : Elementary Methods*. John Wiley & sons, Inc, New York.
2. Alder, B.J., and Wainwright, T.E. J. 1957. Phase Transition for Hard Sphere System. *Journal of Chemical Physics*. 27, 1208-1209.
3. Alder, B.J., and Wainwright, T.E. J. 1959. Studies in molecular dynamics. I. General method. *Journal of Chemical Physics*. 31, 459-466.
4. http://www.ch.embnet.org/MD_tutorial/pages/MD.part1.html
5. Stillinger, F.H, and Rahman, A. 1974. Improved simulation of liquid water by molecular dynamics. *Journal of Chemical Physics*. 60, 1545-1557.
6. Yonezawa, F. 1990. *Molecular Dynamics Simulations*. Springer-Verlag, Berlin Heidelberg New York.
7. Allen, M.P., and D.J. Tildesley. 1987. *Computer Simulation of Liquids*. Clarendon press, Oxford.
8. Goodfellow, J.M. 1995. *Computer Modelling in Molecular Biology*. VCH puplishers, New York.
9. McHaney, R. 1991. *Computer Simulation : A Practical Perspective*. Academic press, Inc, San Diego, California.

10. Case, D.A., Pearlman, D.A., Caldwell, J.W., Cheatham III, T.E., Ross, W.S., Simmerling, C.L., Darden, T.A., Merz, K.M., Stanton, R.V., Cheng, J.J., Vincent, J.J., Crowley, M., Ferguson, D.M., Radmer, R.J., Seibel, G.L., Singh, U.C., Weiner, P.K., and Kollman, P.A. 1997. *AMBER 5*, University of California, San Francisco.

11. Brooks, B.R., Bruccoleri, R.E., Olafson, States, D.J., Swaminathan, S., and Karplus, M. 1983. CHARMM : A Program for Macromolecular Energy Minimization and Dynamics calculation. *Journal of computational Chemistry*. 4, 187-217.

12. Van Gunsteren, W.F., and Berendsen, H.J.C. 1987, *Groningen Molecular Simulation (GROMOS) Library Manual*. Biomos, Nijenborgh 4, 9747 AG Groningen, The Netherlands.

13. Jorgensen, W., and Tirado-Rivers, J. 1988. "The OPLS Potential Functions for Proteins : Energy Minimizations for Crystals of Cyclic Peptides and Crambin". *Journal of American Chemical Society*. 110, 1657-1666.

14. Meijer, L.A., Leermakers, F.A.M., and Lyklema, 1995. Modeling the Interactions between Phospholipid Bilayer Membranes with and without Additives. *Journal of Physical* Chemistry. 99, 17282-17293.

15. Cevc, G. and Marsh, D. 1987. *Phospholipid Bilayer: Physical Principles and Models*. John Wiley & sons, Inc, New York.

16. Saier, Jr. M.H., and Stiles, C.D. 1975. *Molecular Dynamics in Biological Membranes*. Springer-Verlag, New York.

17. Cevc, G. 1993. *Lipid Handbook*. Marcel Dekker, Inc., New York.

18. Small, D.M., Craven, B.M., Lange, G.G., and Steiner, J. 1986. *Handbook of Lipid Research 4: The Physical Chemistry of Lipids*. Plenum Press, New York and Londonh.

19. Pasenkiewicz-Gierula, M., Murzyn, K., Rog, T., and Czaplewski, C. 2000. Molecular Dynamics Simulation Studies of Lipid Bilayer Systems. *Acta Biochimica Polonica*. 47, 601-611.

20. Wong, P.T.T., Siminovitch, D.J., and Mantsch, H.H. 1988. Structure and Properties of Model Membranes: New Knowledge from High-Pressure Vibrational Spectroscopy. *Biochemica et Biophysica Acta*. 947, 139-171.

21. Braganza, L.F, and Worcester, D.L. 1986. Hydrostatic Pressure Induces Hydrocarbon chain Interdigitation in Single-component Phospholipid Bilayers. *Biochemistry*. 25, 2591-2596.

22. Winter, R. and Pilgrim, W.C. 1989. A SANS Study of High Pressure Phase Transitions in Model Biomembranes. *Ber. Bunsengers Phys. Chem*. 93, 708-717.

23. Driscoll, D.A., Jonas, J., and Jonas, A. 1991. High Pressure $^{2}H$ Nuclear Magnetic Resonance study of the Gel Phase of Dipalmitoylphosphatidylcholine. *Chemistry and Physics of Lipid*. 58, 97-104.

24. Moore, P.B., Lopez, C.F., Klein, M.L. 2001. Dynamical Properties of a Hydrated Lipid Bilayer from a Multinanosecond Molecular Dynamics Simulation. *Biophysical Journal*. 81, 2484-2494.

25. Blume, A. 1993. Dynamics Properties. In *Phospholipid Handbook*. Ed. Gregor Ceve. Merecel Dekker, New York. 455-552.

26. Belohorcova, K., Davis, J.H., Woolf, T.B., and Roux, B. 1997. Structure and Dynamics of an Amphiphilic Peptide in a Lipid Bilayer: A Mpllecular Dynamics Study. *Biophysical Journal*. 73, 3039-3055

27. Stouch, T.R. 1993. Lipid Membrance Structure and Dynamics studied by all-atom Molecular Dynamics Simulations of Hydrated Phospholipid Bilayers. *Molecular Simulation*. 10, 335-362.

28. Granek, R. 1997. From Semi-flexible Polymers to Membranes: Anomalous Diffusion and Reptation. *Journal of Physical Chemistry*. 100, 17011-17020.

29. Granek, R., and Pierrat, S. 1999. Enhanced Transverse Diffusion in Active Biomembranes. *Physical Review Letters*. 83, 872-875.

30. Feller, S.E., Venable, R.M., and Pastor, R.W. 1997. "Computer simulation of a DPPC Phospholipid Bilayer: Structural Changes as a Function of Molecular Surface Area". *Langmuir*. 13, 6555-6561.

31. Brooks, C.L., Karplus, M., and Pettitt, B.M. 1988. Proteins: A Theoretical Perspective of Dynamics, Structure and Thermodynamics. In *Advances in Chemical Physics, Vol. LXXI*. Ed. I. Prigogine and S.A. Rice. John Wiley and Sons, New York.

32. Raghavan, M., Reddy, M.R., and Berkowitz, M.L. 1992. A Molecular Dynamics Study of the Structure and Dynamics of Water Between DLPE Bilayers. *Langmuir*. 8, 233-240.

33. Heller, H., Schaefer, M., and Schulten, K. 1993. Molecular Dynamics Simulation of a Bilayer of 200 Lipids in the Gel and in the Liquid Crystal-Phases. *Journal of Physical Chemistry*. 97, 8343-8360.

34. Damodaran, K.V., and Merz, K.M. 1994. A Comparison of DMPC-based and DLPE-based Lipid Bilayers. *Langmuir*. 9, 1179-1183.

35. Tu, K., Tobias, D.J., and Klein, M.L. 1995. Constant Pressure and Temperature Molecular Dynamics Simulation of a Fully Hydrated Liquid Crystal Phase Dipalmitoylphosphatidylcholine Bilayer. *Biophysical Journal*. 69, 2558-2562.

36. Shinoda, W., Fukada, T., Okazaki, S., and Okada, I. 1995. Molecular Dynamics Simulation of the Dipalmitoylphosphatidylcholine (DPPC) Lipid Bilayer in the Fluid Phase Using the Nose-Parrinello-Rahman NPT Ensemble. *Chemical Physics Letters*. 232, 308-312.

37. Zubrzycki, I.Z, Xu, Y., Madrid, M., and Tang, P. 2000. Molecular Dynamics Simulation of a Fully Hydrated Dipalmitoylphosphatidylcholine Membrane in Liquid-Crystal Phase. *Journal of Chemical Physics*. 112 (7), 3437-3441.

38. van der Ploeg, P., and Berendsen, H.J.C. 1982. Molecular dynamics simulation of a bilayer membrane. *Journal of Chemical Physics*. 76, 3271-3276.

39. van der Ploeg, P., and Berendsen, H.J.C. 1980. Molecular Dynamics of Model Membranes. *Biophys. Struct. Mech*. 6, 106.

40. van der Ploeg, P., and Berendsen, H.J.C. 1983. Molecular dynamics of a bilayer membrane. *Molecular Physics*. 49, 233-248.

41. Damodaran, K.V., Kenneth, M., Merz, J., and Gaber, B.P. 1992. Structure and dynamics of the dilauroylphosphatidylethanolamine lipid bilayer. *Biochemistry*. 31, 7656-7664.

42. Egberts, E., and Berendsen, H.J.C. 1988. Molecular Dynamics Simulation of a Smectic Liquid Crystal with Atomic Detail. *Journal of Chemical Physics*. 89, 3718-3732.

43. Egberts, E., Marrink, S.J., and Berendsen, H.J.C. 1994. Molecular dynamics simulation of a phospholipid membrane. *European biophysics journal*. 22. 423-426.

44. Patra, M., Karttunen, M., Hyvonen, M.T., Falck, E., Lindqvist, P., and Vattulainen, I. 2003. Molecular Dynamics Simulations of Lipid Bilayers: Major Artifacts Due to Truncating Electrostatic Interactions. *Biophysical Journal*. 84 (6), 3636-3645.

45. Berger, O., Edholm, O., and Jahnig, F. 1997. Molecular Dynamics Simulations of a Fluid Bilayer of Dipalmitoylphosphatidylcholine at Full Hydration, Constant Pressure, and Constant Temperature. *Biophysical Journal*. 72, 2002-2013.

46. Ayton, G., Smondyrev, A.M., Bardenhagen, S.G., McMurtry, P., and Voth, G.A. 2002. Calculating the Bulk Modulus for a Lipid Bilayer with Nonequilibrium Molecular Dynamics Simulation. *Biophysical Journal*. 83, 1026-1038.

47. Damodaran, K.V., Merz, Jr. K.M., and Gaber, B.P. 1992. Structure and Dynamics of the Dilauroylphosphatidylethanolamine Lipid Bilayer. *Biochemistry*. 31, 7656-7664.

48. Smondyrev, A.M., and Berkowitz, M.L. 1999. Molecular Dynamics Simulation of DPPC Bilayer in DMSO. *Biophysical Journal*. 76, 2472-2478.

49. Marrink, S.J., and Berendsen, H.J.C. 1994. Simulation of water transport through a lipid membrane. *Journal of Physical Chemistry*. 98, 4155-4168.

50. Marrink, S.J., and Berendsen, H.J.C. 1996. Permeation Process of Small Molecules across Lipid Membranes Studied by Molecular Dynamics Simulations. *Journal of Physical Chemistry*. 100, 16729-16738.

51. Lindahl, E., and Edholm, O. 2000. Mesoscopic Undulations and Thickness Fluctuations in Lipid Bilayers from Molecular Dynamics Simulations. *Biophys. J.* 79, 426-433.

52. Zhou, F., and Schulten, K. 1995. Molecular dynamics study of a membrane-water interface. *Journal of Physical Chemistry*. 99, 2194-2208.

53. Kothekar, V. 1996. Molecular Dynamics Simulation of Hydrated Phospholipid Bilayers. *Indian Journal of Biochemistry and Biophysics*. 33, 431-447.

54. Hansen, J.P. and McDonald, J.R. 1976. *Theory of Simple Liquid.* Academic Press, New York.

55. Herman, J., Berendsen, C., and Tieleman, D.P. 1998. Molecular Dynamics: Studies of Lipid Bilayers. In "*Encyclopedia of Computational Chemistry*", vol. 3, ed. Schleyer, P.V.R. John Wiley & Sons, Chichester, New York.

56. Pathria, R.K., 1972. *Statistical Mechanics*. Pergamon Press, Oxford.

57. Maple, J.R., Hwang, M.J., Stockfisch, T.P., Dinur, U, Waldman, M, Ewig, C.S, and Hagler, A.T. 1994. Derivation of Class II Force Fields. I. Methodology and Quantum Force Field for the Alkyl Functional Group and Alkane Molecules. *Journal of Computational Chemistry*. 15. 162-182.

58. Hagler, A.T., and Ewig, C.S. 1994. On the use of Quantum Energy Surfaces in the Derivation of Molecular Force Fields. *Computer Physics Communications*. 84, 131-155.

59. Cornell, W.D., Cieplak, P., Bayly, C.I, Gould, I.R., Merz, Jr. K.M., Ferguson, D.M., Spellmeyer, D.C., Fox, T., Caldwell, J.W., and Kollman, P.A. 1995. A Second Generation Force Field for the Simulation of Proteins, Nucleic Acids, and Organic Molecules. *Journal of American Chemical Society*. 117, 5179-5197.

60. Wipff. G., Dearing, A., Weiner, P.K., Blaney, J.M., and Kollman, P.A. 1983. Molecular Mechanics Studies of Enzyme-Substrate Interactions: The Interaction of L- and D-N-Acetyltryptophanamide with α-Chymotrypsin. *Journal of American Chemical Society*. 105, 997-1005.

61. Kollman, P.A., Weiner, P.K., and Dearing, A. 1981. Studies of Nucleotide Conformations and Interactions: The Relative Stabilities of Double-Helical B-DNA Sequence Isomers. *Biopolymers*. 20, 2583-2621.

62. Weiner, S.J., Kollman, P.A., Case, D.A., Singh, U.C., Ghio, C., Alagona, G, Profeta, Jr. S., and Weiner, P. 1984. A New Force Field for Molecular Mechanical Simulation of Nuclic Acids and Proteins. *Journal of American Chemical Society*. 106, 765-784.

63. MacKerell, A.D, Bashford, D.,Bellott, M., Dunbrack, Jr.R.L., Evanseck, J.D., Field, M.J., Fischer, S., Gao, J., Guo, H., Ha, S., Joseph-McCathy, D., Kuchnir, L., Kuczera, K., Lau, F.T.K., Mattos, C., Michnick, S., Ngo, T., Nguyen, D.T., Prodhom, B., Reiher, W.E., III, Roux, B., Schlenkrich, M., Smith, J.C., Stote, R., Straub, J., Watanabe, M., Wiorkiewicz-Kuczera, J., Yin, D., and Karplus, M. 1998. All-Atom

Empirical Potential for Molecular Modeling and Dynamics studies of Proteins. *Journal of Physical Chemistry B*. 102, 3586-3616.

64. Pettersson, I., and Liljefors, T. 1996. Molecular Mechanics Calculated Conformational Energies of Organic Molecules: A Comparison of Force Fields. In Reviews in Computational Chemistry Volume 9. Ed. Lipkowitz, K.B., and Boyd, D.B. 167-189.
65. Smondyrev, A.M., and Berkowitz, M.L. 1999. United Atom Force Field for Phospholipid Membranes: Constant Pressure Molecular Dynamics Simulation of Dipalmitoylphosphatidicholine/Water system. *Journal of Computational Chemistry*. 20, 531-545.
66. Byrne, P. 1999. *Mplecular Dynamics Simulation of a Fully Hydrated DPPC Bilayer at Varying Hydrostatic Pressure*. Bachelor of Science (Honours) Thesis, Department of Physics, Memorial University of Newfoundland, St.John's, Canada.
67. *COMPASS1.0 Condensed Phase Optimized Molecular Potential f Atomistic Simulation Studies*. 1997. Distributed by Molecular Simulations, Inc.
68. Clementi, E. 1989. *Modern Techniques in Computational Chemistry: MOTECC-89*. ESCOM Science Publishers B.V., Leiden, The Netherlands.
69. Cheng, A., Stanton, R.S., Vincent, J.J., Damodaran, K.V., Dixon, S.L., Hartsough, D.S., Mori, M., Best, S.Aand Merz, Jr.K.M. 1997. *ROAR 1.0*, The Pennsylvania State University.
70. Wheeler, D.R., and Newman, J. 2002. A Lees Expensive Ewald Lattice Sum. *Chemical Physics Letters*. 366, 537-543.

71. Woodcock, L.V. 1971. Isothermal Molecular Dynamic Calculation for Liquid Salt. *Chemical Physics Letters*. 10. 257-261.

72. Berendsen, H.J.C., Postma, J.P.M., Gunsteren, W.F.v., DiNola, A., and Haak, J.R. 1984. Molecular Dynamics with Coupling to External Bath. *Journal of Physical Chemistry*. 81, 3684-3690.

73. Nose, S. 1984. A Molecular Dynamics Method for Simulations in the Canonical Ensemble. *Molecular Physics*. 52 (2), 255-268.

74. Nose, S. 1984. A Unified Formulation of the Constant Temperature Molecular Dynamics Methods. *Journal of Chemical Physics*. 81, 511-519.

75. Hoover, W.G. 1985. Canonical Dynamics: Equilibrium Phase-Space Distributions. Physical Review A. 31, 1695-1697.

76. Martyna, G., and Klein, M.L. 1992. Nose-Hoover Chains: The Canonical Ensemble via Continuous Dynamics. Journal of Chemical Physics. 97, 2635-2643.

77. Parrinello, M., and Rahman, A. 1980. Crystal Structure and Pair Potentials: A Molecular-Dynamics Study. Physical Review Letters. 45, 1196-1199.

78. Martyna, G.J., Tobias, D.J., and Klein, M.L. 1994. Constant Pressure Molecular Dynamics Algorithms. Journal of Chemical Physics. 101, 4177-4189.

79. Cheng, A., and Merz, Jr.K.M. 1996. Application of the Nose-Hoover Chain Algorithm to the Study of Protein Dynamics. *Journal of Physical Chemistry*. 100, 1927-1937.

80. Deng, Z., Martyna, G.J., and Klein M.L. 1994. Quantum Simulation Studies of Metal-ammonia Solutions. *Journal of Chemical Physics*. 100, 7590-

81. *Cerius2 version 2.0*. 1995. Molecular Simulations Inc.

82. Rand, R.P., and Parsegian, V.A. 1989. Hydration Forces between Phospholipid Bilayers. *Biochimica et Biophysica Acta*. 988, 351-376

83. Jorgensen, W.L., Chandrasekhar, J., Madura, J.D., Impey, R.W., and Klein, M.L. 1983. Comparison of Simple Potential Functions for Simulating Liquid. *Journal of Chemical Physics*. 79, 926-

84. Schlenkrich, M., Brickmann, J., MacKerell, A.D., and Karplus, M. 1996. An Empirical Potential Energy Function for Phospholipids: Criteria for Parameter Optimization and Applications. In *Biological Membranes*. Ed. Merz, Jr.K, and Roux, B., Birkhauser, Boston. 31-81

85. Martyna, G., Tuckerman, M.E., Tobias, D.J., and Klein, M.L. 1996. Explicit Reversible Integrators for Extended Systems Dynamics. *Molecular Physics*. 87, 1117-1157.

86. Forester, T.R., and Smith, W. 1998. SHAKE, Rattle, and Roll: Efficient Constraint Algorithms for Linked Rigid Bodies. Journal of Computational Chemistry. 19, 102-111.

87. Nagle, J.F., and Tristram-Nagle, S. 2000. Structure of Lipid Bilayers. *Biochimica et Biophysica Acta*. 1469, 159-195.

88. Tardieu, A., Luzzati, V., and Reman, F.C. 1973. Structure and Polymorphim of the Hydrocarbon Chains of Lipids: A Study of Lecithin-Water Phases. *Journal of Molecular Biology*. 75, 711-733.

89. Lis, L.J., McAlister, M., Fuller, N., Rand, R.P., and Parsegian, V.A. 1982. Interactions between Neutral Phospholipid Bilayer Membranes. *Biophysical Journal.* 37, 657-666.

90. Janiak, M.J., Small, D.M., and Shipley G.G. 1979. Temperature and Compositional Dependence of the Structure of Hydrated Dimyristoyl Lecithin. *Journal of Biological Chemistry.* 254, 6068-6078.

91. Rand, R.P., and Parsegian, V.A. 1989. Hydration Forces Between Phospholipid Bilayers. *Biochimica et Biophysica Acta.* 988, 351-376

92. Nagle, J.F., Zhang, R., Tristram-Nagle, S., Sun, W.S., Petrache, H.I., and Suter, R.M. 1996. X-ray Structure Determination of Fully Hydrated $L_\alpha$ Phase DPPC Bilayer. *Biophysical Journal.* 70, 1419-1431.

93. Sun, W.S., Suter, R.M., Knewtson, M.A., Worthington, C.R., Tristram-Nagle, S., Zhang, R., and Nagle, J.F. 1994. Order and Disorder in Fully Hydrated Unoriented Bilayers of Gel Phase Dipalmitoylphosphatidylcholine. *Physical Review E.* 49, 4665-4676.

94. Buldt, G., Gally, U., and Seelig, J. 1979. Neutron Diffrection Studies on Phosphatidylcholine Model Membranes I: Head Group Conformation. *Journal of Molecular Biology.* 134, 673

95. Tristram-Nagle, S., Zhang, Suter, R.M., Worthington, C.R., Sun, W.J., and Nagle, J.F. 1993. Measurement of Chain Tilt Angle in Fully Hydrated Bilayers of Gel Phase Lecithins. *Biophysical Journal.* 64, 1097-1109.

96. Driscoll, D.A., Samarasinghe, S., Adamy, S. Jonas, J., and Jonas, A. 1991. Pressure Effects on Dipalmitoylphosphatidylcholine Bilayers Measured by 2H Nuclear Magnetic Resonance. Biochemistry. 30. 3322-3327.

97. Morrow, M.R., and Lu, D. 1991. Universal Behavior of Acyl Chain Order: Chain Length Scaling. Chemical Physics Letters. 182. 435-439.

98. Seelig, A., and Seelig, J. 1974. The Dynamic Structure of Fatty Acyl Chains in a Phospholipid Bilayer Measured by Deuterium Magnetic Resonance. Biochemistry. 13, 4839-4845.

99. Shinoda, W., Namiki, N., and Okazaki, S. 1997. Molecular Dynamics Study of a Lipid Bilayer: Convergence, Structure, and Long-time Dynamics. Journal of Chemical Physics. 106. 5731-5743.

100. Feller, S.E., Yin, D., Pastor, R.W., and Mackerell, Jr. A.D. 1997. Molecular Dynamics Simulation of Unsaturated Lipid Bilayer at Low Hydration: Parameterization and Comparison with Diffraction Studies. *Biophysical Journal*. 73, 2269-2279.

# APPENDICES

## Appendix A: Molecular Dynamics Simulation Control Inputs

**Input parameters for energy minimization with ROAR program**

```
$cntrl
        imin=1,maxcyc=500,ncyc=100,imgslt=0,iftres=1,
        cut=13,scee=1.0,scnb=1.0,kmax=12,ntpr=50,ntb=1,ntx=1,
        ntt=1
 $end
eof
```

**Input parameters for molecular dynamics simulation with ROAR program**

```
$cntrl
        imin=0,nrun=500,nstlim=500,dt=0.001,imgslt=0,iftres=1,
        cut=13,scee=1.0,scnb=1.0,kmax=6,ntpr=50,ntb=2,ntx=13,
        ntt=1,init=4,ntorp=4,nchain=1,mtstat(1)=5,pext=1000,
        temp0=323,tempi=323,ntf=3,ntc=3,tol=0.0005,ntwx=500,ntwv=500,
        ntwe=50,nhcprnt=1,qfactor=12.000,wfactor=1.200
 $end
eof
```

# Appendix B: H′, Temperature and Pressure Variation at 1 atm and 423 K

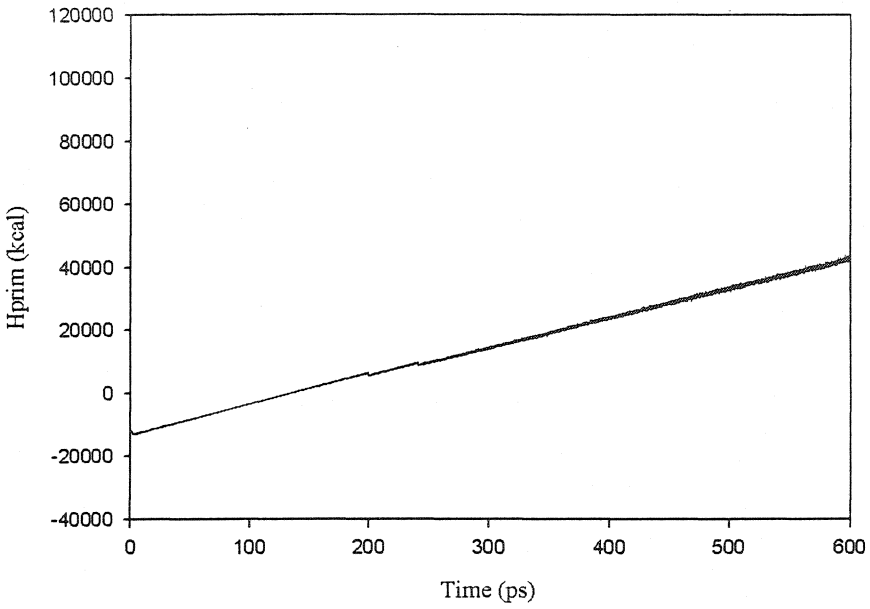


Figure B.1: H′ as a function of time for the DPPC bilayer simulation at 323 K temperature and 1 atm pressure

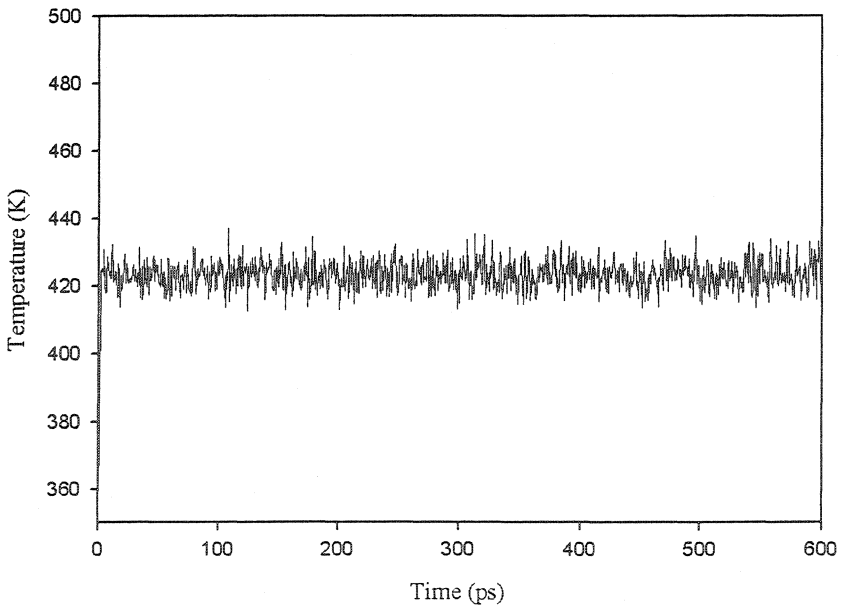


Figure B.2: System temperature as a function of time for the DPPC bilayer simulation at 423 K and 1 atm

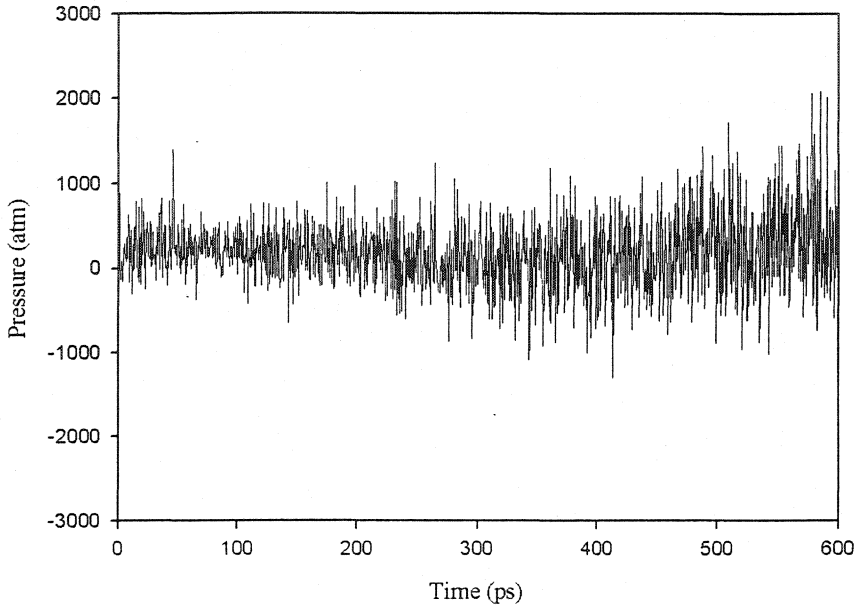


Figure B.3: System Pressure as a function of time for the DPPC bilayer simulation at 423 K and 1 atm

## Appendix C: H′, Temperature and Pressure Variation at 1000 atm and 323 K

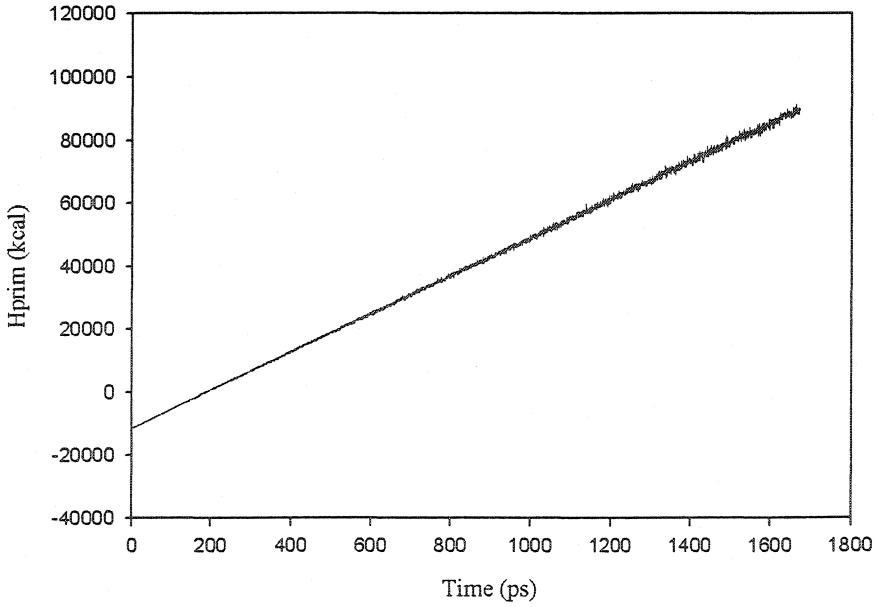


Figure C.1: H′ as a function of time for the DPPC bilayer simulation at 323 K temperature and 1 atm pressure

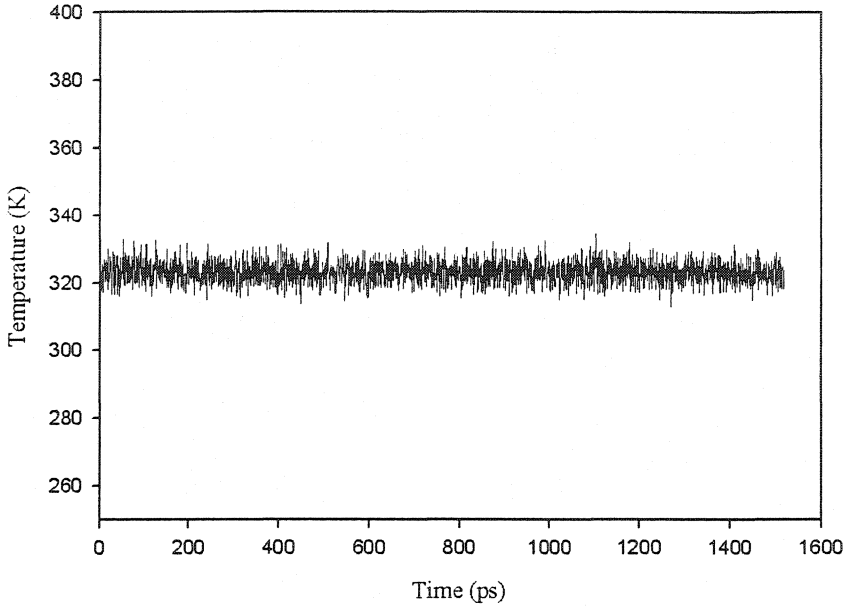


Figure C.2: System temperature as a function of time for the DPPC bilayer simulation at 323 K and 1000 atm

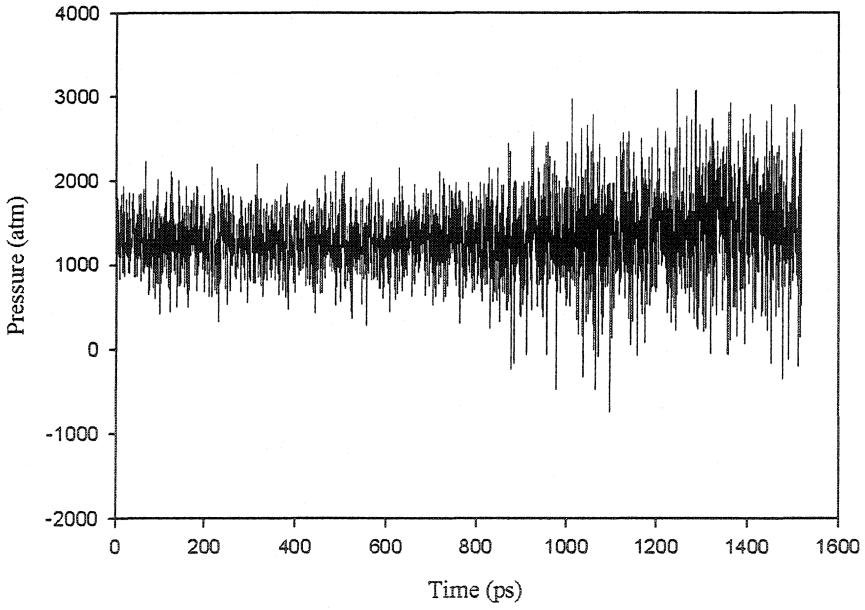


Figure C.3: System Pressure as a function of time for the DPPC bilayer simulation at 323 K and 1000 atm

# Appendix D: H′, Temperature and Pressure Variation at 2000 atm and 323 K

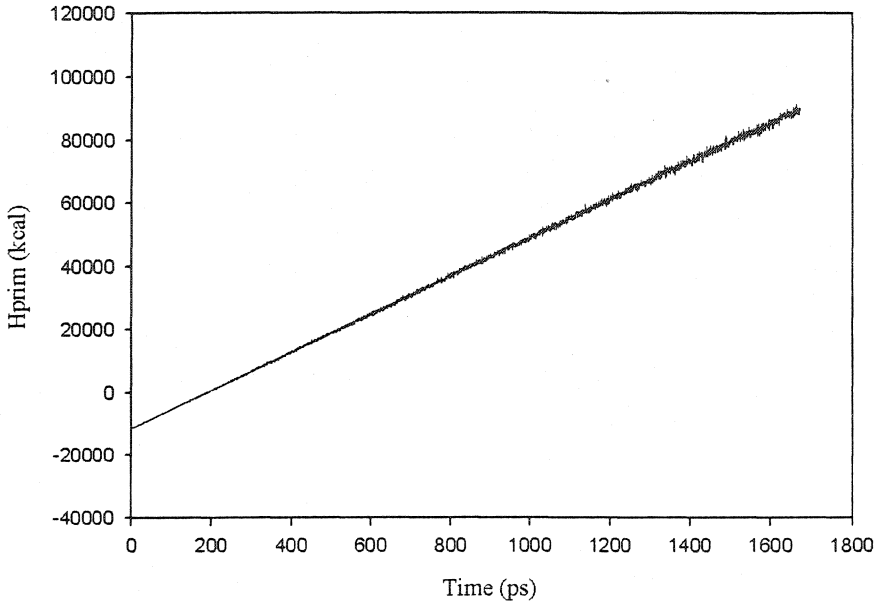


Figure D.1: H′ as a function of time for the DPPC bilayer simulation at 323 K temperature and 1 atm pressure

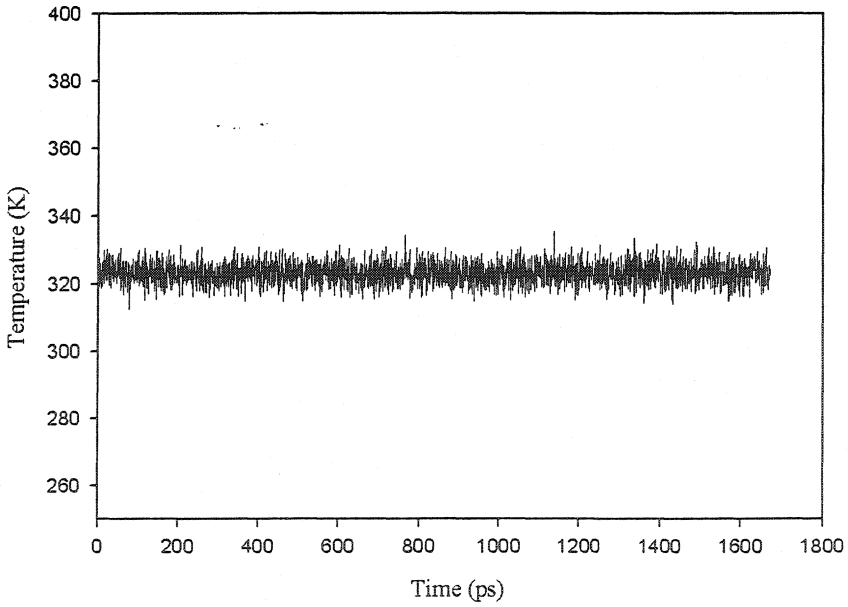


Figure D.2: System temperature as a function of time for the DPPC bilayer simulation at 323 K and 2000 atm

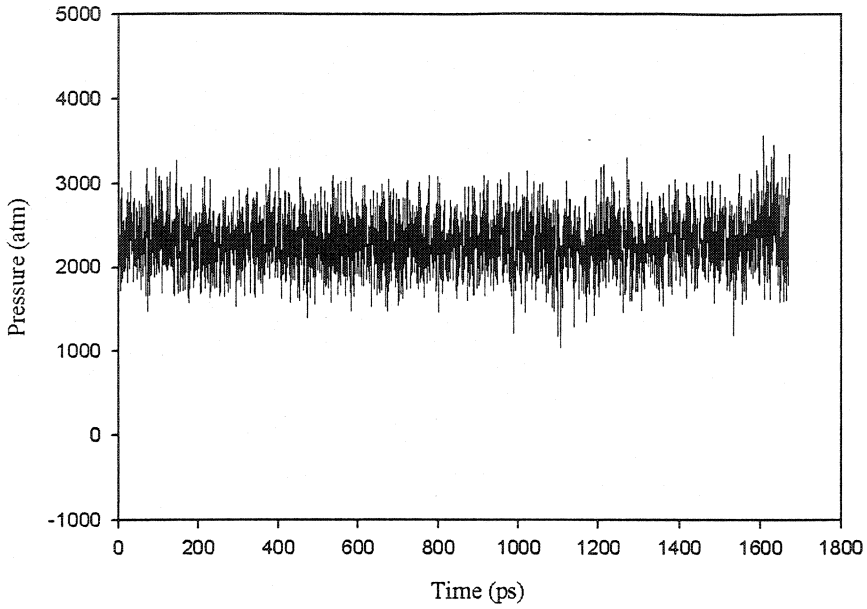


Figure D.3: System Pressure as a function of time for the DPPC bilayer simulation at 323 K and 2000 atm

## **Appendix E**: Initial DPPC Bilayer System

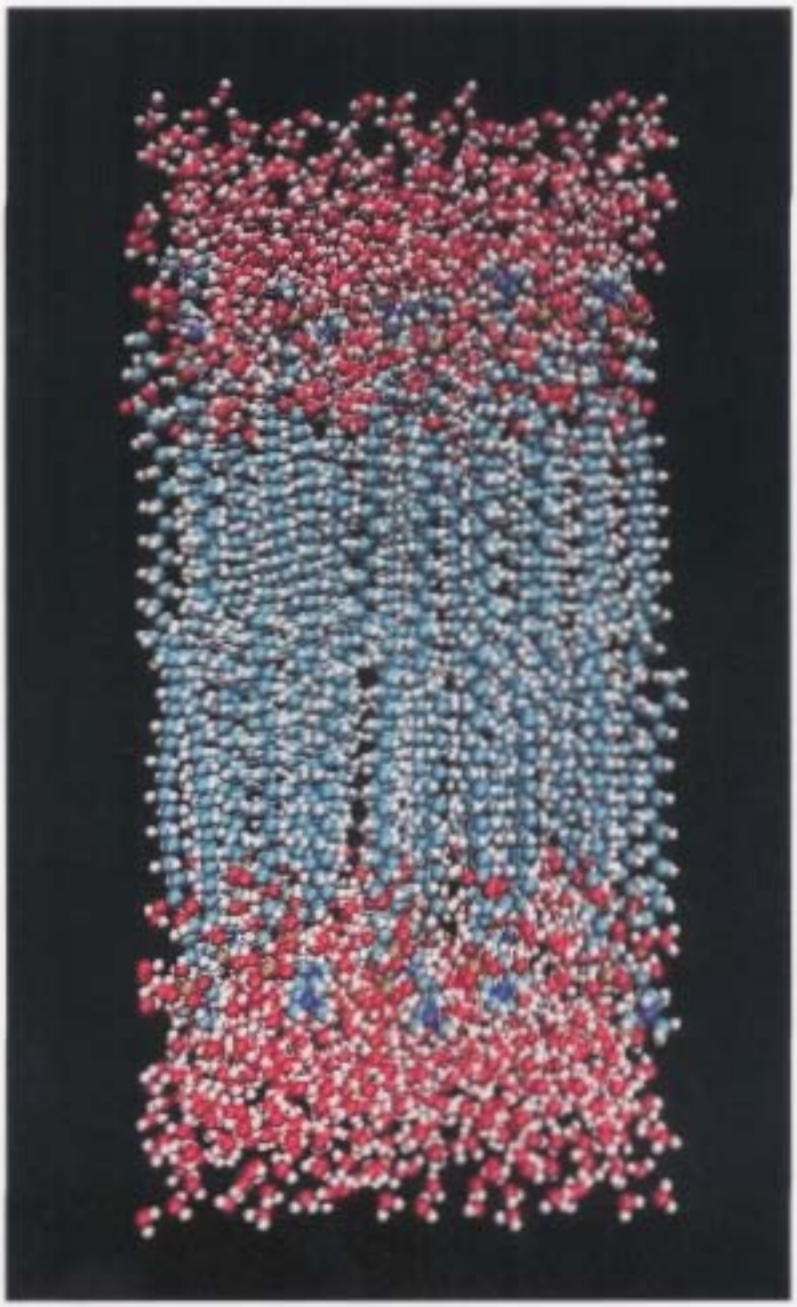

## Appendix F: Final DPPC Bilayer System at 1 atm Pressure and 323 K Temperature

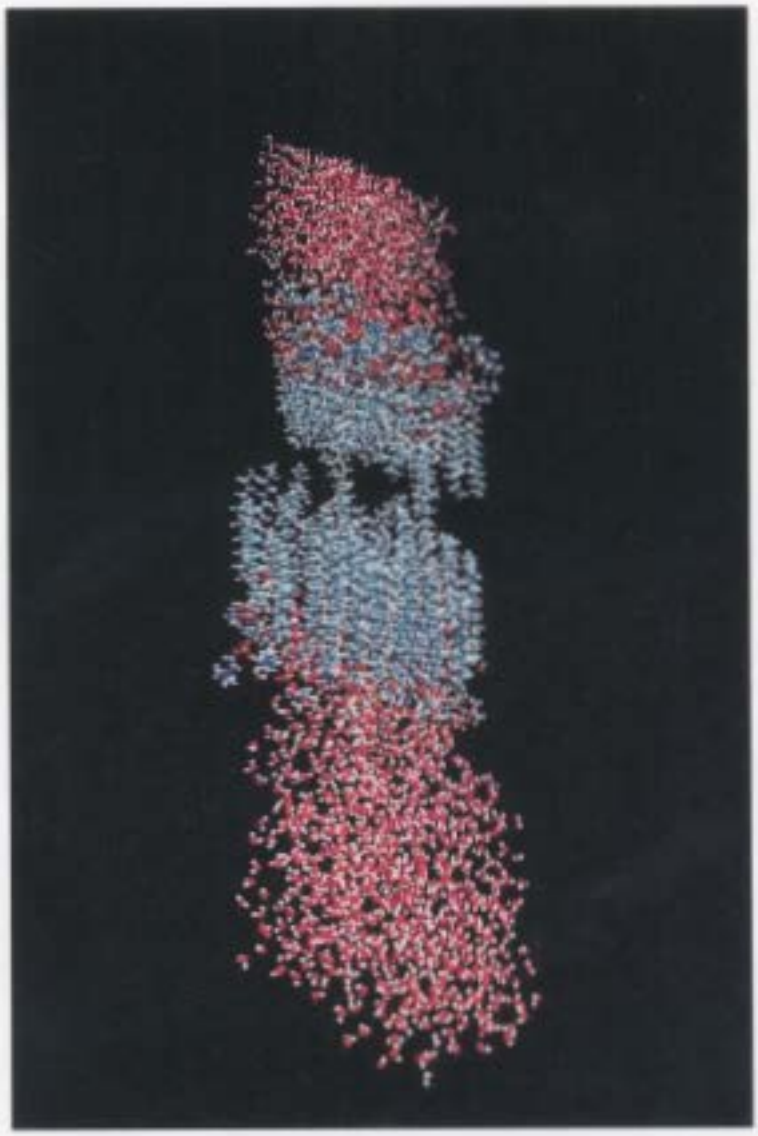

## Appendix G: Final DPPC Bilayer System at 1 atm Pressure and 423 K Temperature

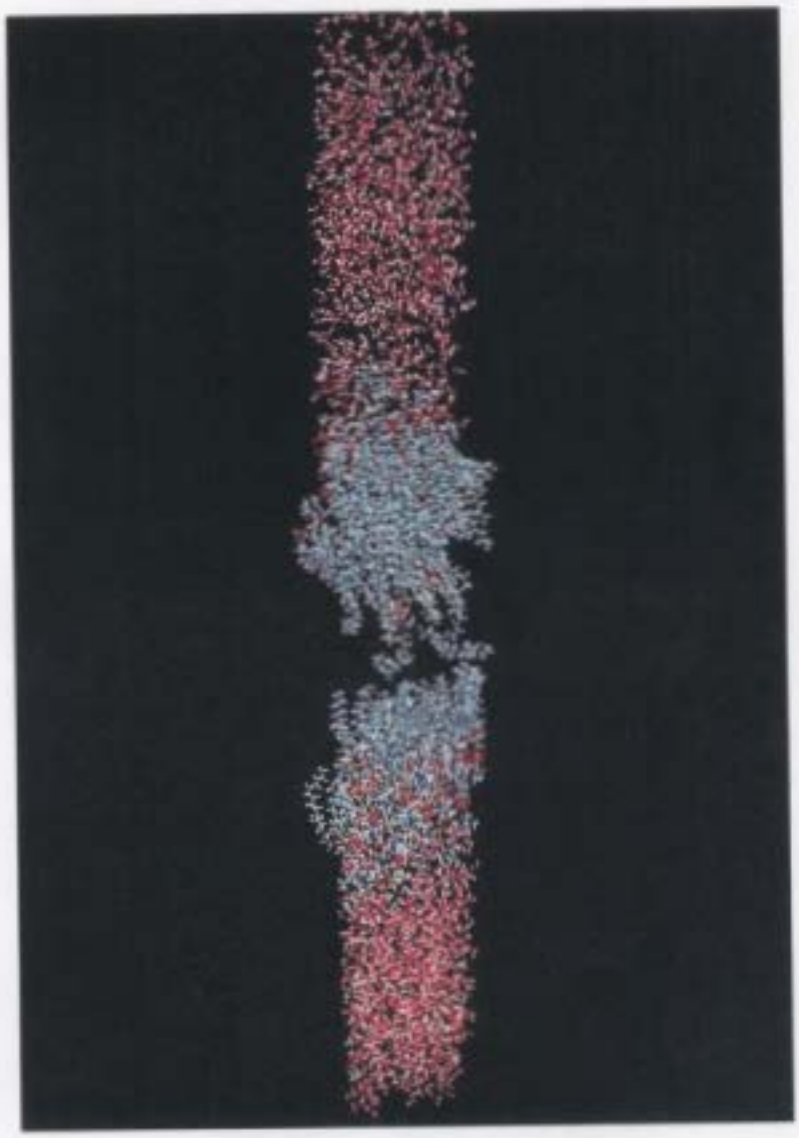

## Appendix H: Final DPPC Bilayer System at 1000 atm Pressure and 323 K Temperature

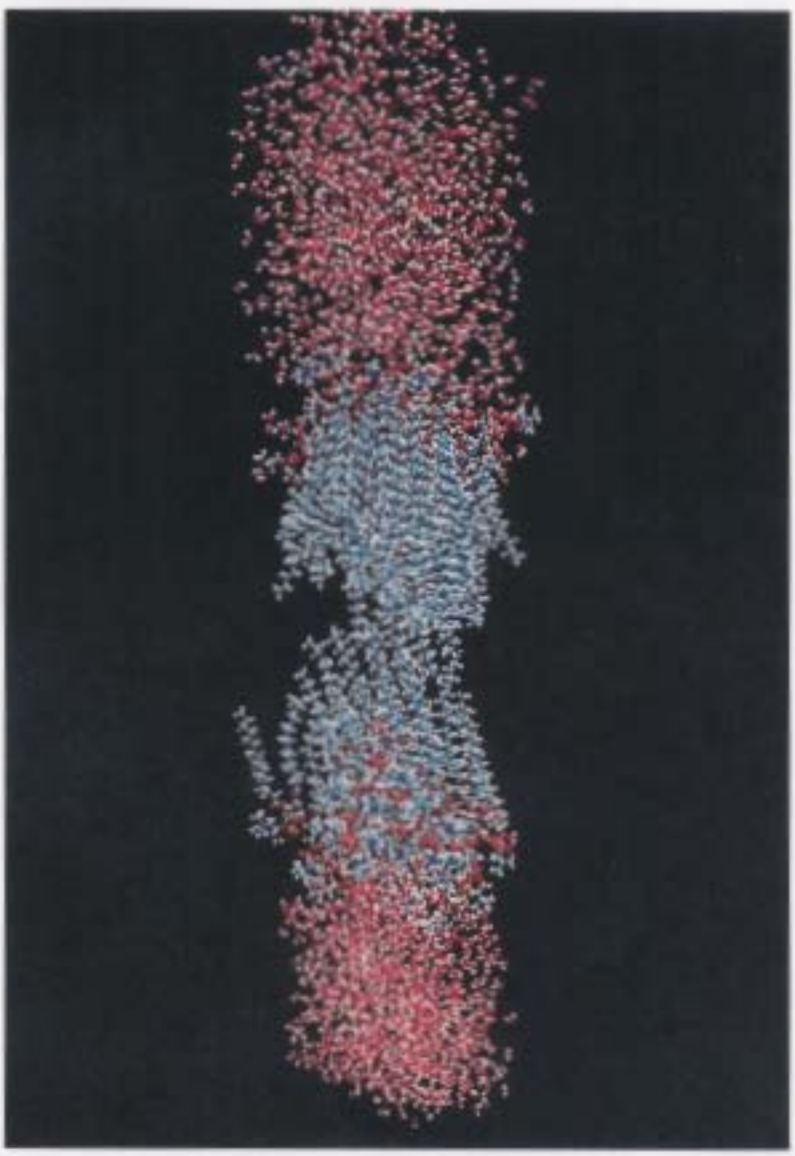

## Appendix I: Final DPPC Bilayer System at 2000 atm Pressure and 323 K Temperature